Chapter 2

Phosphonate ester functionalized imidazolium salts and their application in organocatalytic aerobic esterification of benzaldehyde

Abstract: A simple organocatalytic technique for oxidative esterification of aromatic aldehydes to esters with boronic acid and alcohols has been investigated. This chapter describes NHC catalysts made with an NHC ligand incorporating a hemilabile ligand. The prepared catalysts are characterized by elemental analysis, FT-IR, ^{1}H, ^{13}C and ^{31}P NMR. Density functional theory calculations are carried out to study electronic nature of the N-heterocyclic carbenes generated from the phosphonate functionalized imidazolium salts. The catalytic efficacy of the phosphonate functionalized imidazolium salts in aerobic esterification of benzaldehyde with aryl boronic acid and aliphatic/aromatic alcohol are investigated. The probable mechanism of the NHC catalysed esterification reaction involving aryl boronic acid is investigated by using theoretical calculations.

2.1. Introduction

In recent years, N-heterocyclic carbenes (NHCs) have provided a window of opportunity for the development of innovative catalytic methods [1-8]. Due to their propensity to coordinate with carbon-electrophiles, NHCs have emerged as potent organocatalysts in different carbon-carbon and carbon-heteroatom bond formation reactions [1-50]. The majority of these catalytic processes are initiated by the carbene's nucleophilic attack on carbonyl groups present in organic substrates. The nucleophilic attack of NHCs on aldehydes reverse the polarity of carbonyl carbon atom and thereby facilitate a diversified array of NHC organocatalyzed reactions. Although the mechanism of such reactivity reversal was not well recognized at the time, the first example of this type of transformation was reported in 1943 by Ugai and coworkers, who reported the homodimerization of aldehydes to benzoins catalysed by a thiazolium salt [3]. The mechanism of this procedure, as proposed by Breslow in 1958, is based on the amphiphilic character of an NHC active catalyst formed in situ from the thiazilium precatalyst [4]. Attack of NHC on carbonyl carbon atom forms an enaminol intermediate presently known as the Breslow intermediate where the original aldehydic carbon atom becomes nucleophilic. The remarkable ability of NHCs to reverse the conventional mode of reactivity of aldehydes is fundamental to many of these reactions (umpolung). Depending upon the identity of carbonyl species, NHC catalysed reactions involving Breslow intermediate operate through distinct reactive species such as acyl anion, homoenolate, and enolate equivalents, which are typically formed by oxidation state reorganisation [5-10]. The homoenolate and enolate equivalents generated by NHC catalysis are nucleophilic entities while acyl azolium and, α,β-unsaturated acyl azoliums are electrophilic cationic entities with unique and unprecedented chemistry [12-13]. Thus, NHCs can catalyse a wide range of organic transformations and many of these reactions are of fundamental importance in organic synthesis. Most notable among these reactions are Benzoin condensation, Stetter reaction, cycloaddition reactions and enolate chemistry of α-functionalized aldehydes (Scheme 2.1) [19-27].

Apart from the above, N-heterocyclic carbene promoted organocatalytic reaction involving Breslow intermediate are widely explored in esterification of benzaldehyde with a varied range of functionalities. The first example of NHC catalysed esterification of benzaldehyde was reported by Miyashita et. al in 1997, where benzimidazolium or

thiazolium salts catalyse direct esterification of aromatic aldehydes into the corresponding esters in presence of a suitable base
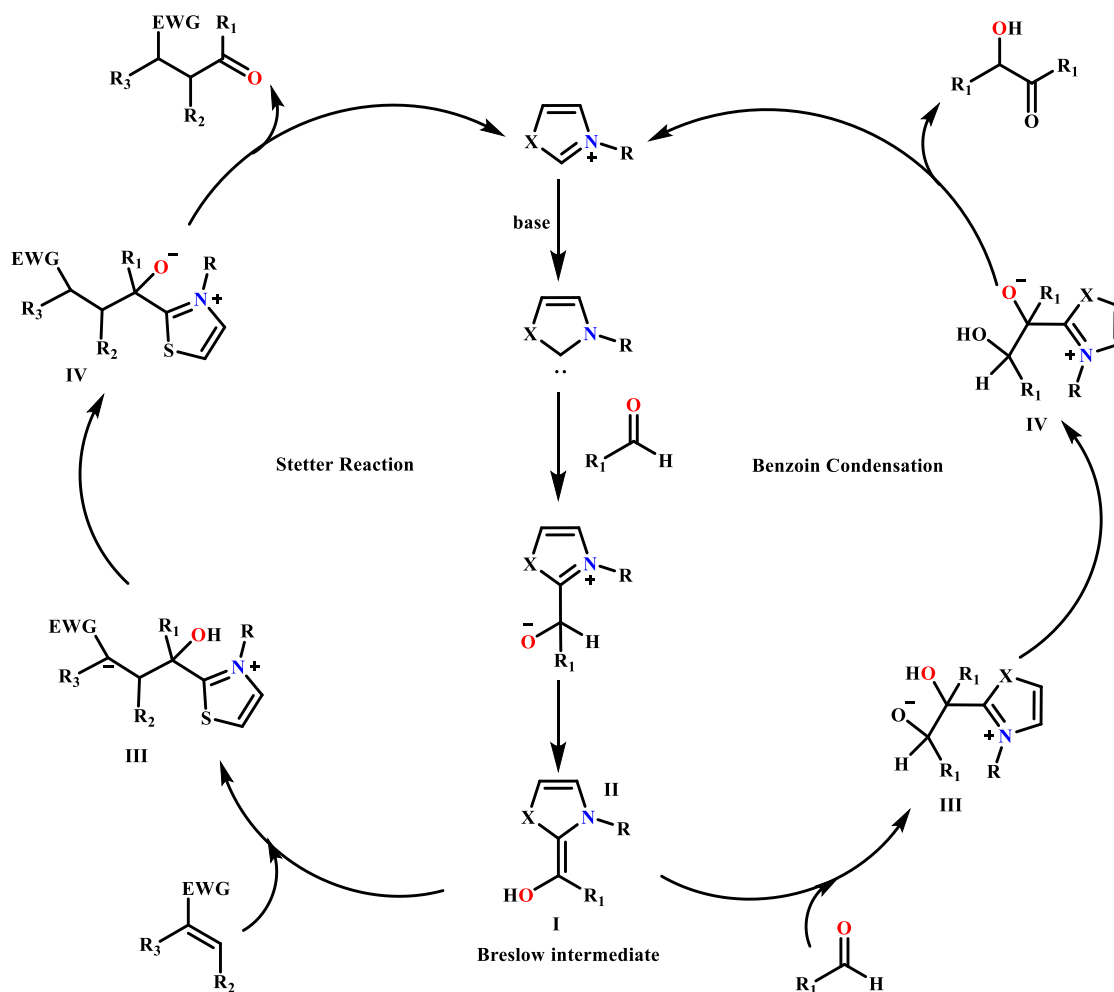
Scheme 2.1. Mechanism of NHC catalysed Benzoin Condensation and Stetter reaction proposed by Breslow and Stetter

e.g. DBU and an oxidant e.g. nitrobenzene [28]. However, the mechanism of this reaction was not well understood and the involvement of NHC in this reaction is not realized until 2007 when Scheidt *et al.* reported NHC catalysed oxidative esterification of aldehydes into the corresponding esters by employing MnO_2 as the oxidant [29]. Subsequent studies explored the utility of a varied range of oxidants and azolium salts in this esterification reaction involving both activated as well as inactivated aldehydes. Moreover, the NHC catalysed esterification of benzaldehyde proceed even when molecular oxygen is used as oxidant and the mechanism of this reaction is slightly different from the one involving use of oxidants like MnO_2 (Scheme 2.2) [38,41].
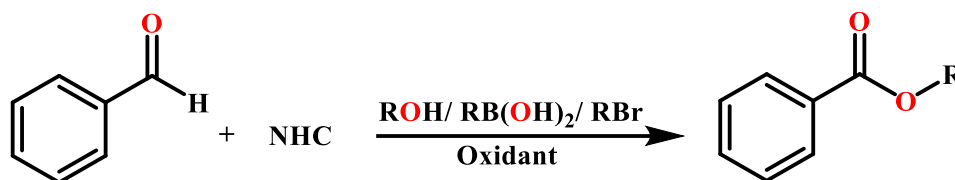
Scheme 2.2. NHC catalysed esterification of benzaldehyde with different substrates

Over the last two decades, NHC catalysed reactions have been explored by employing imidazolium, triazolium and thiazolium salts as NHC precursors while large number of studies also focused on augmenting the catalytic efficacy by tuning the substituents present in these heterocycles [30-50]. Among these, thiazolium and triazolium precursors have emerged as the preferred choice as precatalyst for NHC catalysed reactions owing to the high catalytic efficacy and tunability associated with these precursors. While imidazolium salts containing sterically less bulky substituents on the imidazole N atoms show poor organocatalytic efficacy, presence of sterically bulky and electron donating aromatic substituents considerably augmented their catalytic efficacy. Nevertheless, easy synthetic possibility to introduce different functional groups on the N-substituent of imidazolium salts provide a versatile route introduce different ancillary functionality on NHCs and offer a unique opportunity to enhance their catalytic efficacy [5-8]. Indeed, complexes bearing donor functionalized NHC ligands are expected to exhibit superior catalytic efficacy because of the hemilabile property [51]. In this regard, NHCs bearing additional donor functionality have been explored though their organocatalytic activity is not very well investigated. Even though, carboxylate or sulphonate functionalized NHCs are reported, phosphonate ester or phosphonic acid functionalized NHCs are yet to be reported [51]. Presence of three O atoms attached to P atom in a phosphonate ester or phosphonic acid moiety render these functionalities highly relevant in design of donor functionalized NHCs. Moreover, the phosphonic acid functionality show strong coordination ability to a host of metal ions and therefore phosphonic acid functionalized NHCs can be possibly used as precursors for heterogenization of NHC catalyst. Thus, we endeavoured to develop phosphonate functionalized NHCs and the synthesis, characterization and organocatalytic behaviour of a series of phosphonate functionalized imidazolium salts are described in this chapter. Apart from that, the electronic characteristics of the NHCs derived from the phosphonate ester functionalized NHCs are explored by employing density functional theory (DFT) calculations.

2.2. Materials and Methods

Starting materials were purchased from commercial sources and used without further purification. Solvents were purified by conventional techniques and distilled prior to use. Infrared spectra were recorded on a Nicolet Impact I-410 FT-IR spectrometer as KBr diluted discs and a Perkin Elmer MIR-FIR FT-IR spectrometer. The progress of the reaction was monitored by thin layered chromatography (TLC) using aluminium sheets with silica gel 60F254 (Merck). UV light was used as a visualising agent. NMR spectra were recorded on a JEOL JNM-ECS400 NMR spectrometer operating at 400 MHz and samples were dissolved in deuterated solvents. Chemical shifts were reported in parts per million downfield of Me_4Si (TMS) as internal standard. The High-Performance Liquid Chromatography (HPLC) spectra were recorded on a UV-Visible Detection-2489, Refractive Index Detector-2414, HPLC Pump-515.

2.2.1. Crystallography

Single crystals of the compound suitable for diffraction measurements were used directly from the reaction mixtures. The diffraction data for both the complexes were collected on a Bruker APEX-II CCD Diffractometer using MoKα radiation (λ=0.71073 Å) using φ and ω scans of narrow (0.5°) frames at 100 K. The structures were solved by direct methods and refinement were carried out using full matrix least squares on F^2 using SHELXL-97 as implemented in the WinGX program system [52]. Anisotropic refinement was executed on all non-hydrogen atoms. The aliphatic and aromatic hydrogen atoms were placed on calculated positions but allowed to ride on their parent atoms during subsequent cycles of refinements.

2.2.2. Computational Details

Structures of the synthesized NHC isomers were modelled using the molecular building and visualization tool Gauss View and geometry optimization was done using the Gaussian 09 software program [53]. Energy minimization along with frequency calculations of the four NHC isomers each corresponding to the singlet, triplet and protonated states were done employing the B3LYP (Becke-3 Parameter-Lee-Yang-Parr) functional and 6-31+G(d,p) basis set for all atoms, without imposing any symmetry constraints [54-55]. Natural Bond Orbital (NBO) calculations were performed at the same level of theory. Absence of imaginary frequencies (NMIAG=0) confirmed the

structures to be true minima on the PES. Zero-point-corrected energies were considered for calculation of relative stabilities, singlet-triplet energy gaps and proton affinities.

2.3. Experimental

2.3.1. Synthesis of 1-mesityl-1H-imidazole (**1**)

1-mesityl-1H-imidazole (**1**) was prepared by flowing a slightly modified version of an earlier reported procedure [56]. Glacial acetic acid (10 mL), aqueous formaldehyde (3mL), and aqueous glyoxal (4.6 mL) were transferred to a round bottom flask (100 mL) and heated at 70 °C. A solution of glacial acetic acid (10 mL), ammonium acetate in water (3.08 g/2 mL), and mesitylamine (5.6 mL) was added drop-wise to the flask over a period of 30 min. The resultant solution was continuously stirred and heated at 70 °C for 18 h. The reaction mixture was then cooled to room temperature and added drop-wise to an aqueous solution of $NaHCO_3$ (1.2 M, 300 mL solution), resulting in precipitation of the product. The precipitate was isolated by vacuum filtration and washed several times with water. The product 1-mesityl-1H-imidazole was obtained as brown solid. [Yield: 2.23 g (73 %), Elemental analysis % found (calculated for $C_{12}H_{14}N_2$): C: 77.26 % (77.38 %) H: 7.50 % (7.58 %) N: 14.98 % (15.04 %), m.p.: (80-95) °C. ^{1}H NMR ($CDCl_3$, 400 MHz, δ/ppm): δ= 7.41 (m, 1H), 7.21 (m, 1H), 6.95 (m, 2H), 6.87 (m, 1H), 2.31 (s, 3H), 1.96 (s, 6H)]**.**

2.3.2. Synthesis of 1-(4-chlorophenyl)-1H-imidazole (**2**)

To a solution of glacial acetic (10 mL), aqueous formaldehyde (3 mL) and aqueous glyoxal (4.6 mL) at 70 °C, was added p-chloroaniline (2.5 g) in CH_3OH (10 ml), glacial acetic acid (10 mL) followed by ammonium acetate in water (3.08 g/2 mL) dropwise over a period of 30 mins. The reaction mixture was stirred at reflux for 18 h at 70 °C. a yellowish mixture was formed. The reaction mixture was then cooled to room temperature and added dropwise to a stirred solution of $NaHCO_3$ (29.4 g in 300 mL water), resulting in precipitation of the product. The precipitate was isolated by vacuum filtration and washed several times with water. The product 1-(4-chlorophenyl)-1H-imidazole was obtained as off white solid. [Yield: 1.578 g (63 %), Elemental analysis % found (calculated for $C_9H_7ClN_2$): C: 60.46 % (60.52 %) H: 3.91 % (3.95 %) N: 15.62 % (15.68 %); m.p.: (65-70) °C. FT-IR (KBr, cm^{-1}): υ 3419(br), 3109(m), 1890(w), 1645(w),

1506(s), 1304(s), 829(s), 661(m). ^{1}H NMR (CDCl$_3$, 400 MHz, δ/ppm): δ= 7.82 (s, 1H), 7.45 (s, 2H), 7.35 (s, 2H), 7.25 (s, 1H), 7.22 (s, 1H)].

2.3.3. Synthesis of 1-(4-bromophenyl)-1H-imidazole (**3**)

A solution of glacial acetic acid (10 mL), aqueous formaldehyde (3 mL) and aqueous glyoxal (4.6 mL) was heated at 70 °C. A mixture of glacial acetic acid (10 mL), p-bromoaniline (6.86 g) in CH$_3$OH (10 mL), and ammonium acetate in water (3.08 g/2 mL) was added dropwise to the flask over a period of 30 mins (dropping funnel). The resulting mixture was then stirred at reflux for 18 h. The mixture was cooled to room temperature and added dropwise to a stirred solution of NaHCO$_3$ (29.4 g in 300 ml water). The precipitate was isolated by vacuum filtration and washed several times with water. Pure yellow colour solid was obtained. [Yield: 2.23 g (72 %), Elemental analysis % found (calculated for C$_9$H$_7$BrN$_2$): C: 48.38 % (48.46 %) H: 3.10 % (3.16 %) N: 12.51 % (12.56 %); m.p.: (85-90) °C. FT-IR (KBr, cm^{-1}): υ 3434(br), 3108(m), 1890(w), 1642(w), 1504(s), 1303(s), 825(s), 661(m). ^{1}H NMR (CDCl$_3$, 400 MHz, δ/ppm): δ= 7.84 (s, 1H), 7.63 (s, 2H), 7.29 (s, 2H), 7.25 (s, 1H), 7.22 (s, 1H)].

2.3.4. Synthesis of 1-(4-nitrophenyl)-1H-imidazole (**4**)

To a solution of aqueous formaldehyde (3 mL) and aqueous glyoxal (4.6 mL) in glacial acetic acid (10 mL) at 70 °C, a mixture of p-nitroaniline (2.756 g) in CH$_3$OH (10 mL), ammonium acetate in water (3.08 g/2 mL) and glacial acetic (10 mL) was added dropwise over a period of 30 mins. The reaction mixture was stirred at reflux for 18 h at 70 °C. The solution was cooled down to room temperature and added dropwise to a stirred solution of NaHCO$_3$ (29.4 g in 300 mL water), resulting in precipitation of the product. The precipitate was isolated by vacuum filtration and washed several times with water. 1-(4-nitrophenyl)-1H-imidazole was obtained as bright yellow solid. [Yield: 1.578 g (80 %), Elemental analysis % found (calculated for C$_9$H$_7$N$_3$O$_2$): C: 57.09 % (57.14 %) H: 3.67 % (3.73 %) N: 22.17 % (22.21 %); m.p.: (165-170) °C. FT-IR (KBr, cm^{-1}): υ 3368(br), 3108(m), 1922(w), 1599(w), 1534(s), 1514(s), 1306(s), 854(s). ^{1}H NMR (CDCl$_3$, 400 MHz, δ/ppm): δ= 8.40 (s, 2H), 7.98 (s, 1H), 7.60 (s, 2H), 7.38 (s, 1H), 7.26 (s, 1H)]

2.3.5. Synthesis of 3-(2-(diethoxyphosphoryl)ethyl)-1-mesityl-1H-imidazol-3-ium-bromide (**5**)

A solution of 1-mesityl-1H-imidazole (2 mmol, 372.5 mg) in tetrahydrofuran (THF) (10 mL) was transferred to a round bottom flask (100 mL). A solution of diethyl-2-bromoethyl phosphonate (1.8 mmol, 441 mg) in THF (10 mL) was added drop-wise to the above solution under N_2 atomsphere and the resulting mixture was refluxed for 24 h. The reaction mixture was then cooled to room temperature and solvent was removed under reduced pressure. The residue was washed with hexane (6 x 10 mL) to remove excess imidazole and the remaining oily residue was dissolved in dichloromethane (10 mL). Extraction using H_2O (3 x 10 mL) and evaporation of solvent in a water bath yielded the product as a light yellow oil. [Yield: 2.182 g (95 %); Elemental analysis % found (calculated for $C_{18}H_{28}BrN_2O_3P$): C: 50.06 % (50.13 %) H: 6.48 % (6.54 %) N: 6.46 % (6.50 %). FT-IR (KBr, cm^{-1}): υ 3433(b), 1640(m), 1460(m), 1204(m), 1159(m), 1037(m), 855(w), 760(w). ^{1}H NMR (400 MHz, CDCl$_3$, δ/ppm): δ= 9.83 (1H, Im-H), 8.19 (1H, Im-H), 7.12 (1H, Im-H), 6.84 (2H,Ar-H), 4.81-4.77 (2H,-N-CH$_2$), 3.97 (4H, -CH$_2$), 2.58-2.54 (2H, -P-CH$_2$), 1.93 (6H, -CH$_3$), 1.15 (9H, Ar-CH$_3$). ^{13}C NMR (100 MHz, CDCl$_3$, δ/ppm): δ= 141.11(Im, N-C-N), 140.13 (C^{Ar}), 137.82 (C^{Ar}), 137.72(C^{Ar}), 134.72 (C^{Ar}), 130.74(C^{Ar}), 129.74(C^{Ar}), 129.42(Ar, N-C), 124.36(Im, C), 123.02(Im, C), 62.64(2C-O), 44.87(C^{Im-N}), 27.50-26.10 (C-P), 17.61 (Ar-C),16.43(C). ^{31}P NMR (CDCl$_3$, δ/ppm): δ= 26.85]

2.3.6. Synthesis of 1-(4-chlorophenyl)-3-(2-(diethoxyphosphoryl)ethyl)-1H-imidazol-3-ium bromide (**6**)

1-(4-chlorophenyl)-1H-imidazole was dissolved in THF under nitrogen. To this solution diethyl-2-bromoethyl phosphonate was added dropwise and refluxed for 24 h under N_2 condition. The reaction mixture was then cooled to room temperature and solvent was removed under reduced pressure. The residue was washed with hexane (6 x 10 mL) to remove excess imidazole and the remaining oily residue was dissolved in dichloromethane (10 mL). Extraction using H_2O (3 x 10 mL) and evaporation of solvent in a water bath yielded the product as a colorless oil. [Yield: 0.555g (78 %); Elemental analysis % found (calculated for $C_{15}H_{21}ClN_2O_3P$): C: 52.39 % (52.41 %) H: 6.08 % (6.16 %) N: 8.09 % (8.15 %). FT-IR (KBr, cm^{-1}): υ 3436(br), 2920(s), 1722(s), 1539(m), 1473(m), 1384(m), 1041(s), 831(w), 707(w). ^{1}H NMR (400 MHz, CDCl$_3$, δ/ppm): δ= 10.90 (1H, Im-H), 7.94 (1H, Im-H), 7.77 (2H,Ar-H), 7.64 ppm (1H, Im-H), 7.56 (2H,

Ar-H), 4.89-4.86 (2H,-N-CH$_2$), 4.13 (4H, -CH$_2$), 2.72-2.68 (2H, -P-CH$_2$), 1.31 (6H, -CH$_3$). ^{13}C NMR (100 MHz, CDCl$_3$, δ/ppm): δ= 136.41(Im, N-C-N), 132.99 (Ar, N-C), 130.72 (C^{Ar}), 124.28(C^{Ar}), 123.50 (C^{Ar}), 120.42(Im, C), 116.11(Im, C), 62.69, 45.07, 29.66 (C-P), 16.35. ^{31}P NMR (CDCl$_3$, δ/ppm): δ= 25.53]

*2.3.7. Synthesis of 1-(4-bromophenyl)-3-(2-(diethoxyphosphoryl)ethyl)-1H-imidazol-3-ium bromide (**7**)*

1-(4-bromophenyl)-1H-imidazole was dissolved in THF. A solution of diethyl-2-bromoethyl phosphonate (1.8 mmol, 441 mg) in THF (10 mL) was added drop-wise to the above solution under N$_2$ atmosphere and the resulting mixture was refluxed for 24 h. The reaction mixture was then cooled to room temperature and solvent was removed under reduced pressure. The residue was washed with hexane (6 x 10 mL) to remove excess imidazole and the remaining oily residue was dissolved in dichloromethane (10 mL). Extraction using H$_2$O (3 x 10 mL) and evaporation of solvent in a water bath yielded the product as a light yellow oil. [Yield: 0.472 g (75%); Elemental analysis % found (calculated for C$_{15}$H$_{21}$Br$_2$N$_2$O$_3$P): C: 38.43 % (38.49 %) H: 4.48 % (4.52 %) N: 5.92 % (5.98 %). FT-IR (KBr, cm^{-1}): υ 3436(br), 2920(s), 1722(s), 1539(m), 1473(m), 1384(m), 1041(s), 831(w), 707(w). ^{1}H NMR (400 MHz, CDCl$_3$, δ/ppm): δ= 11.17 (1H, Im-H), 7.82 (1H, Im-H), 7.73 (2H,Ar-H), 7.69 ppm (2H, Ar-H) 7.49 (1H, Im-H) 4.91-487 (2H,-N-CH$_2$), 4.13 (4H, -CH$_2$), 2.70-2.67 (2H, -P-CH$_2$), 1.31 (6H, -CH$_3$). ^{13}C NMR (100 MHz, CDCl$_3$, δ/ppm). δ= ^{13}C NMR (100 MHz, CDCl$_3$, δ/ppm): δ= 136.41(Im, N-C-N), 132.78 (Ar, N-C), 132.48 (C^{Ar}), 123.49(C^{Ar}), 122.70 (C^{Ar}), 123.29(Im, C), 119.16(Im, C), 61.71, 44.11, 28.68 (C-P), 15.42. ^{31}P NMR (CDCl$_3$, δ/ppm): δ= 25.53]

*2.3.8. Synthesis of 3-(2-(diethoxyphosphoryl)ethyl)-1-(4-nitrophenyl)-1H-imidazol-3-ium bromide (**8**)*

In an oven-dried round bottom flask, 1-(4-nitrophenyl)-1H-imidazole was dissolved in THF. To this was added diethyl-2-bromoethyl phosphonate was added dropwise. The resulting mixture was stirred at reflux for 24 h under nitrogen atmosphere. The reaction mixture was then cooled to room temperature and solvent was removed under reduced pressure. The residue was washed with hexane (6 x 10 mL) to remove excess imidazole and the remaining oily residue was dissolved in dichloromethane (10 mL). Extraction using H$_2$O (3 x 10 mL) and evaporation of solvent in a water bath yielded the product as a light yellow oil. [Yield: 0.571 g (83 %); Elemental analysis % found (calculated for C$_{15}$H$_{21}$BrN$_3$O$_5$P): C: 41.44 % (41.49 %) H: 4.76 % (4.87 %) N: 9.62 % (9.68 %). FT-IR

(KBr, cm^{-1}): υ 3436(br), 2920(s), 1722(s), 1539(m), 1473(m), 1384(m), 1041(s), 831(w), 707(w). ^{1}H NMR (400 MHz, CDCl$_3$, δ/ppm): δ= 11.02 (1H, Im-H), 8.45 (2H,Ar-H), 8.17 (2H, Ar-H), 8.01(1H, Im-H), 7.72 ppm (1H, Im-H), 4.88-4.84 (2H,-N-CH$_2$), 4.16 (4H, -CH$_2$), 3.71 (2H), 3.11 (6H), 2.73-2.70 (2H, -P-CH$_2$), 1.31 (6H, -CH$_3$). ^{13}C NMR (100 MHz, CDCl$_3$, δ/ppm): δ= 148.30 (NO$_2$-C^{Ar}), 138.88 (Ar, N-C), 137.12 (Im, N-C-N), 125.99 (C^{Ar}), 124.62 (C^{Ar}), 123.25 (C^{Ar}), 123.25 (Im, C), 120.37 (Im, C), 62.79, 31.90, 29.67 (C-P), 16.36. ^{31}P NMR (CDCl$_3$, δ/ppm): δ= 25.39]

2.3.9. Typical procedure for oxidation of aromatic aldehydes to aryl esters using boronic acid

Aromatic aldehyde (0.65 mmol) was added to a suspension of boronic acid (0.5 mmol), **5-8** as catalyst and caesium carbonate (0.75 mmol) in toluene (10 mL) at room temperature. The reaction mixture was refluxed at 70 °C under open atmosphere until the completion of the reaction. The reaction progress was monitored by using thin layer chromatography (TLC). After completion of the reaction, the reaction mixture was filtered through a pad of celite, eluted with ethyl acetate (10 ml) and dried over anhydrous Na$_2$SO$_4$. The solvent was removed by using the rotavapor and the collected residue were purified through a silica gel column. Ethyl acetate/hexane mixture was used as the eluent. Percentage conversions were determined using HPLC techniques and percentage conversion were calculated using internal standard.

*2.3.10. Typical procedure for oxidation of aromatic aldehydes to aryl esters using alcohols*

A solution of p-substituted benzaldehyde (0.65 mmol) and alcohols (1.9 mmol) in toluene (5 ml) was added to a suspension of imidazolium catalyst (**5-8**) (0.023 g) and caesium carbonate (0.75 mmol) dissolved in toluene (5ml) at 70 °C temperature for 12 h. After completion of the reaction, the reaction mixture was filtered through a pad of celite®, washed with ethyl acetate (10 mL), and dried over anhydrous Na$_2$SO$_4$. Under reduced pressure, the solvent was evaporated, and the remaining substance was purified using a silica gel column using ethyl acetate/hexane mixture as eluent. HPLC techniques were used to calculate percentage conversions by adding internal standard.

2.4. Results and Discussion

2.4.1. Synthesis and characterization of N-substituted imidazoles

Reaction of different anilines with glyoxal and paraformaldehyde in presence of ammonium acetate yielded four differently substitute N-aryl imidazole's (Scheme 2.3). All the four N-aryl imidazole products were characterized by using FT-IR, ^{1}H NMR and

^{13}C NMR studies. Single crystal X-ray diffraction measurements unequivocally established the molecular structures of the 4-mesityl, 4-chloro and 4-bromophenyl substitutes imidazole's.
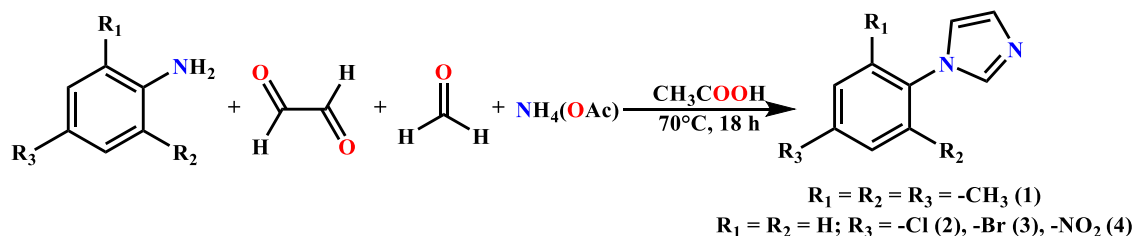
Scheme 2.3. Synthesis of N-aryl substituted imidazole **1-4**

The FT-IR spectrum of all four N-aryl imidazole's (**1-4**) are depicted in Figure 2.1. Aromatic C-H stretching vibrations of **1-4** appear as strong peaks in the range 3125-3094 cm^{-1} while aliphatic C-H stretching vibration of methyl groups in **1** are observed as strong bands centered at 2977-2920 cm^{-1}. C-H bending vibration of **1-4** appear in the range of 1939-1890 cm^{-1}. The C=N stretching frequency of **1-4** is observed at 1650-1599 cm^{-1}. The prominent peak at 1514 cm^{-1} is attributed to the N=O stretching frequency of compound **4**.
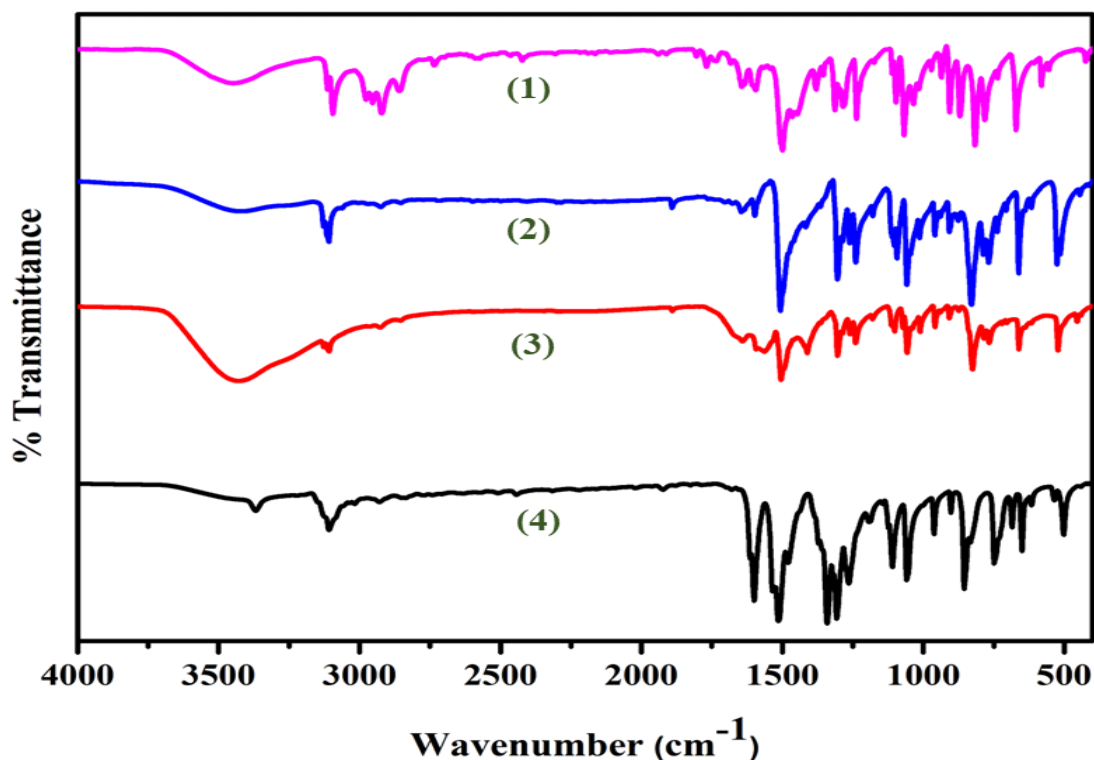
Figure 2.1. FT-IR spectra of N-aryl imidazole's (**1-4**)

The peaks observed in the range of 1498-1534 cm^{-1} can be attributed to C=C stretching band of the aromatic rings of **1-4.** The strong peak at the range of 1313-1303 cm^{-1} is indicative of the C-N stretching frequency of **1-4**. The C-Cl band stretching frequency shows a prominent peak at 829 cm^{-1} of compound **2**. The sharp peak at 661 cm^{-1} corresponds to the C-Br stretching frequency of compound **3**.

The ^{1}H NMR spectra of all four N-aryl imidazole's (**1-4**) are shown in Figure 2.2. Peaks for all the constituent protons in **1-4** are observed in expected chemical shifts in the ^{1}H NMR spectra of **1-4**. Ortho and para substituted methyl protons of N-mesityl imidazole (**1**) resonate at 1.96 and 2.31 ppm, respectively. The aromatic proton attached to the C2 carbon atom of imidazole ring in **1-4** are observed as singlets at δ 7.41, 7.82, 7.84 and 7.98 ppm, respectively. The other aromatic protons of the imidazole ring and the N-aryl substituents are observed in the range 8.40-6.87 ppm and conform well with the expected formulations of the N-aryl imidazoles.
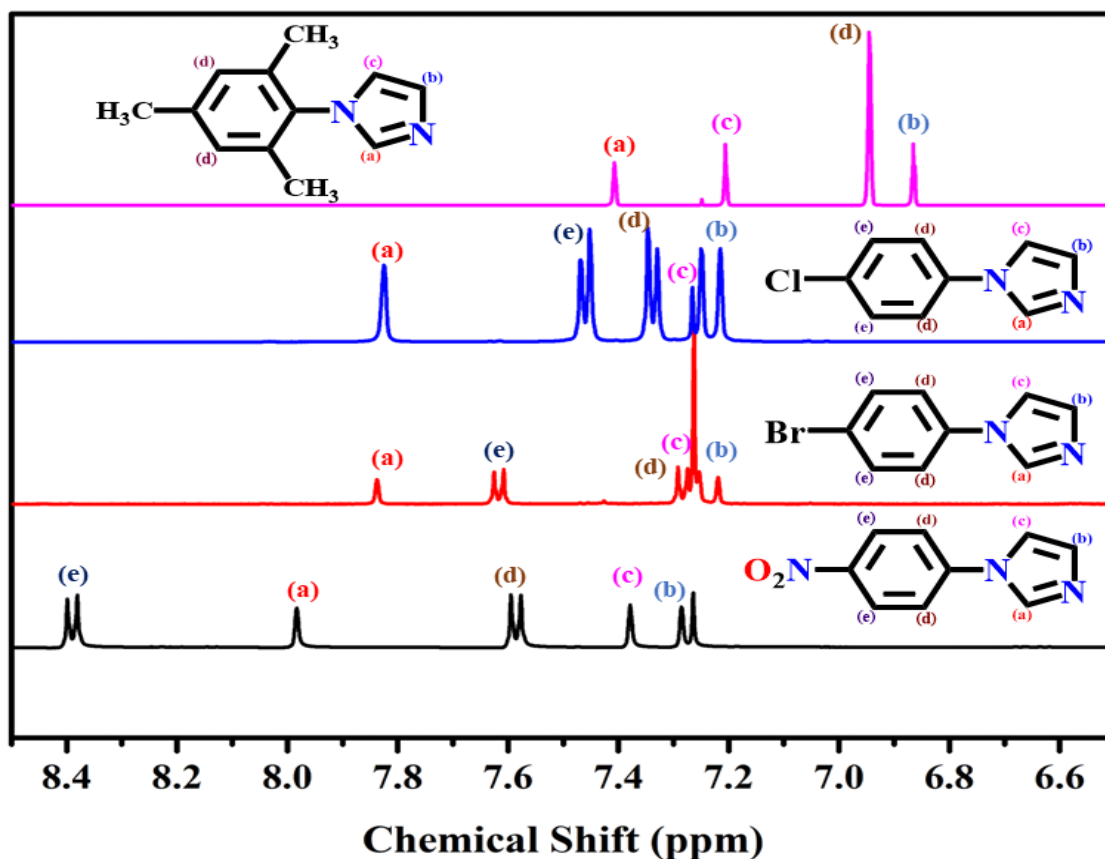
Figure 2.2. ^{1}H NMR spectra of N-aryl imidazoles (**1-4**)

The ^{13}C NMR spectra of N-aryl imidazole's (**1-4**) are depicted in Figure 2.3. The same trend as for ^{1}H NMR spectra were found for the ^{13}C NMR spectra. The signals of the aromatic carbon atoms of **1-4** are sharp. Herein, the characteristics signals for imidazole C2 at δ 135.49, 135.54, 135.49 ppm and 135.41 ppm provide compelling evidence validating the identity of compounds (**1-4**). Additionally, distinctive signals for C-belonging to methyl group for compound **1** at 17.39 ppm, 21.11 ppm and the phenyl group observed at (117.66-146.31) ppm corroborate to the fact that anticipated compounds (**1-4**) have been synthesized accordingly.
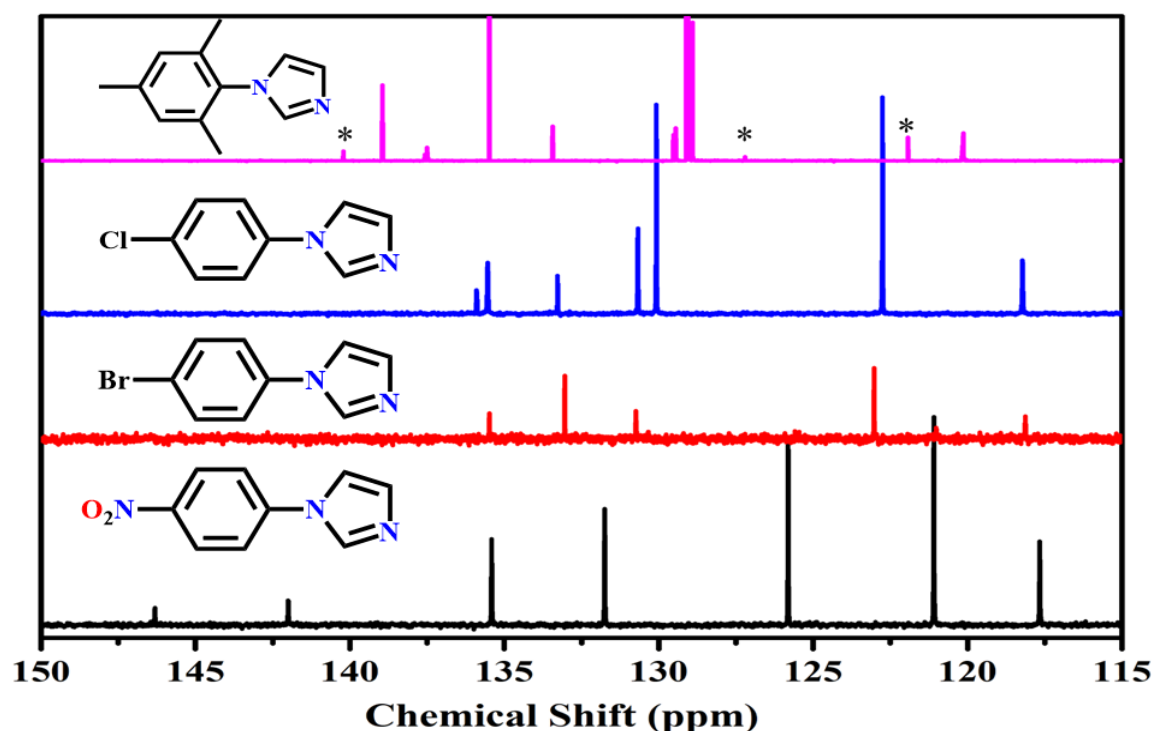
Figure 2.3. ^{13}C NMR spectra of N-aryl imidazoles (**1-4**)

2.4.2. Single crystal X-ray structures of N-substituted imidazoles (**1-3**)

The molecular structures of N-aryl substituted imidazoles (**1-3**) were determined through single crystal X-ray diffraction analysis. Compound **1** crystallizes in orthorhombic *P*na2$_1$ space group while compounds **2** and **3** crystallize in monoclinic *P*2$_1$/c space group. Molecular structures of **1-3** depicted in Figure 2.4 unambiguously establish formation of the N-aryl substituted imidazoles. Relevant crystal data along with refinement parameters of **1-3** are listed in Table 2.1 while selected bond lengths and bond angles are listed in Table 2.2. All the bond lengths and bond angles in compounds **1-3** are in good agreement with values typically observed in earlier reported N-aryl substituted imidazoles.
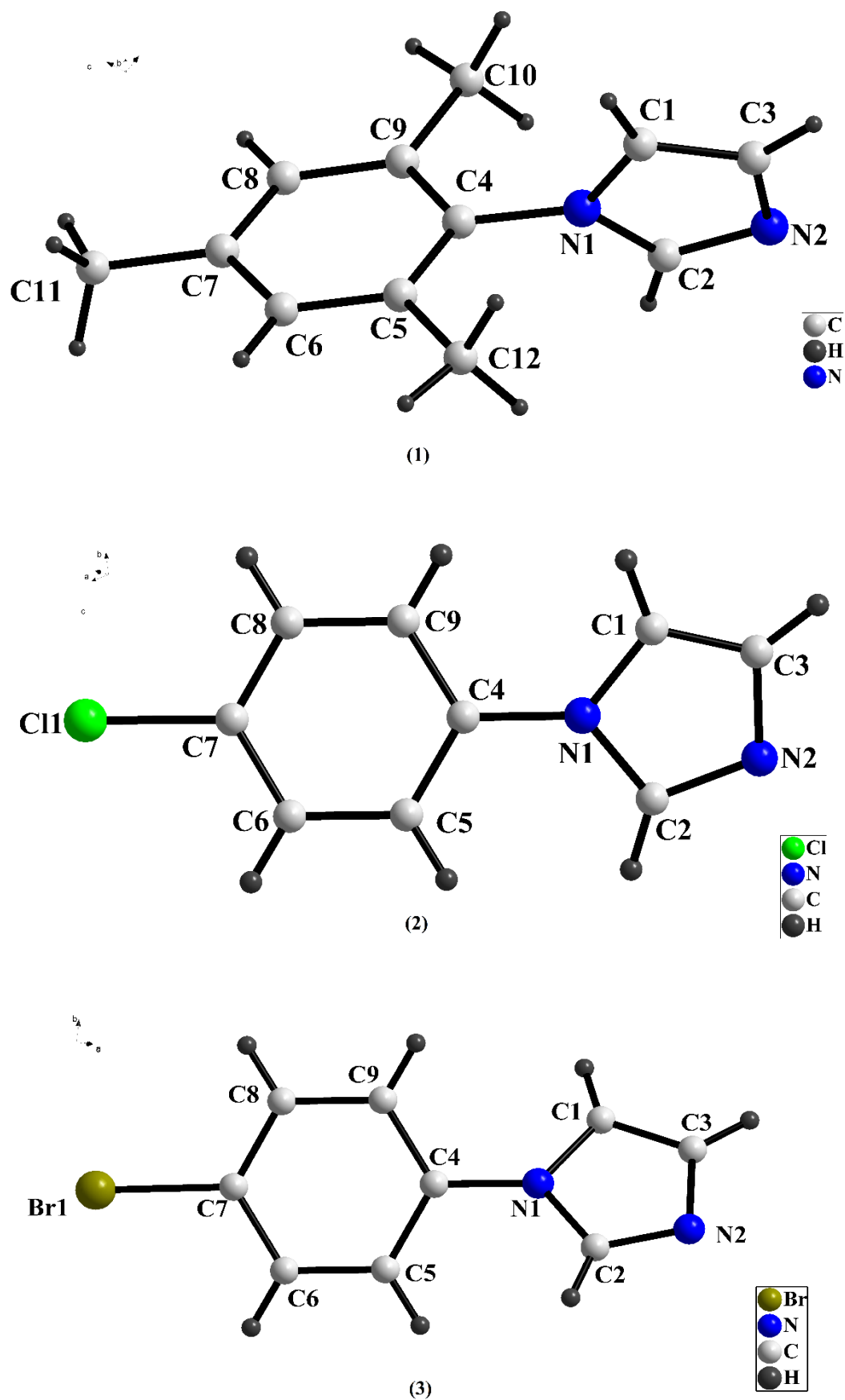
(1)

(2)

(3)

Figure 2.4. Molecular structures of N-aryl imidazoles (**1**-**3**)

However, for compound **2**, the N(2)-C(2)-N(1) bond angle is found to be significantly smaller as compared to corresponding angles observed in **1** and **3**. Also, the same trend is indicated by C(2)-N(2) bond length which is considerably longer for compound **2**.

Table 2.1. Crystal data and refinement parameters of **1-3**

| Compounds	**1**	**2**	**3**
Empirical formula	$C_{24}H_{28}N_4$	$C_{2.57}H_2Cl_{0.29}N_{0.57}$	$C_9H_7BrN_2$
Formula weight	372.50	51.03	223.08
Temperature	296(2) K	296(2) K	373(2) K
Wavelength	0.71073 Å	0.71073 Å	0.71073 Å
Crystal system	Orthorhombic	Monoclinic	Monoclinic
Space group	$Pna2_1$	$P2_1/c$	$P2_1/c$
a	10.5693(10) Å	8.118(9) Å	7.9992(17) Å
b	9.3405(9) Å	11.229(13) Å	11.338(2) Å
c	10.9239(10) Å	9.226(11) Å	9.238(2) Å
α	90°	90°	90°
β	90°	99.32(3)°	97.648(4)°
γ	90°	90°	90°
Volume	1078.44(18) $Å^3$	829.9(16) $Å^3$	830.4(3) $Å^3$
Z	2	14	4
Density (calculated) ρ_{calc}	1.147 Mg/m^3	1.430 Mg/m^3	1.784 Mg/m^3
Absorption coefficient (μ)	0.069 mm^{-1}	0.398 mm^{-1}	4.888 mm^{-1}
F(000)	400	368	440
Crystal size mm^3	0.55 x 0.10 x 0.10	0.60 x 0.10 x 0.10	0.70 x 0.10 x 0.10
Theta range for data collection	2.869 to 28.105°	2.543 to 28.408°	2.569 to 29.061°
Reflections collected	8612	13697	33089
Independent reflections	2575 [R(int) = 0.0640]	2069 [R(int) = 0.1249]	2188 [R(int) = 0.0747]
Completeness to theta = 25.242°	99.9 %	100.0 %	100.0 %
Data / restraints / parameters	2575 / 1 / 127	2069 / 0 / 109	2188 / 0 / 109
Goodness-of-fit on F2	0.936	1.008	1.038
Final R indices [I>2sigma(I)]	R1 = 0.0639, wR2 = 0.1500	R1 = 0.0821, wR2 =0.1990	R1 = 0.0225, wR2 = 0.0495
R indices (all data)	R1 = 0.1221, wR2 = 0.1868	R1 = 0.1657, wR2 =0.2526	R1 = 0.0343, wR2 = 0.0524

Moreover, due to the presence of bulky ortho-methyl substituents in **1**, the mean planes containing the aromatic carbon atoms of the mesityl ring and the plane containing the atoms of imidazole ring are almost perpendicular to each other. The angle between these two planes are reasonably smaller in case of **2-3** due to the absence of any such substituents on the ortho position of the N-aryl substituents.

Table 2.2. Selected bond lengths [Å] and bond angles [°] of **1-3**

Bonds Lengths [Å]	1	2	3
N(1)-C(1)	1.377(5)	1.364(5)	1.383(2)
N(1)-C(2)	1.354(5)	1.365(5)	1.370(2)
N(1)-C(4)	1.437(5)	1.417(5)	1.427(2)
C(3)-C(1)	1.353(6)	1.287(5)	1.361(2)
C(3)-N(2)	1.357(6)	1.360(6)	1.382(2)
C(2)-N(2)	1.306(5)	1.365(6)	1.320(2)
Cl(1)-C(7)	-	1.741(4)	-
Br(1)-C(7)	-	-	1.9004(18)
C(2)-N(1)-C(1)	105.8(3)	105.1(3)	106.61(15)
C(2)-N(1)-C(4)	126.3(3)	127.4(3)	126.82(15)
C(1)-N(1)-C(4)	127.8(3)	127.5(3)	126.52(15)
C(2)-N(2)-C(3)	103.9(4)	109.5(4)	104.73(15)
C(1)-C(3)-N(2)	112.0(4)	105.8(3)	111.08(16)
N(2)-C(2)-N(1)	113.2(4)	106.6(4)	111.98(16)
C(5)-C(4)-N(1)	119.3(3)	120.3(4)	119.32(16)
C(9)-C(4)-N(1)	118.8(3)	119.9(3)	120.11(16)

*2.4.3. Synthesis of phosphonate ester functionalized imidazolium salts (**5-8**)*

Phosphonate ester functionalized imidazolium salts (**5-8**) were synthesized by treatment of equimolar amount of N-aryl imidazoles (**1-4**) with diethyl-2-bromoethyl phosphonate in tetrahydrofuran (THF) (Scheme 2.4). The desired phosphonate ester functionalized imidazolium salts (**5-8**) were obtained in good yields. All the products (**5-8**) were characterized using elemental analysis, FT-IR, NMR spectroscopy and high-resolution mass spectrometry (HR-MS).
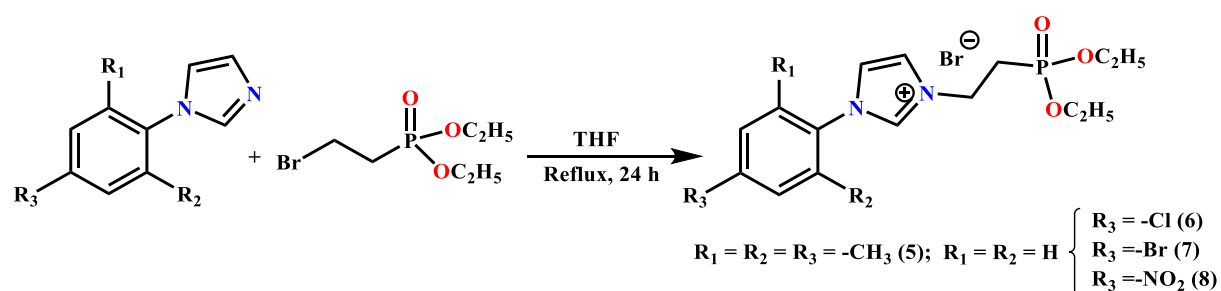
Scheme 2.4. Synthesis of phosphonate ester functionalized imidazolium salts **5-8**

The FT-IR spectra of phosphonate ester functionalized imidazolium salts (**5-8**) are depicted in the Figure 2.5. Intense peaks observed in the range 2991-2848 cm^{-1} can be attributed to C-H stretching vibrations in (**5-8**) while C=N stretching vibrations are observed in the range 1640-1690 cm^{-1}. Bands observed between 1530-1551 cm^{-1} correspond to aromatic C=C stretching vibrations while prominent peaks at 1350-1392 cm^{-1} can be attributed to C-N stretching vibrations. Characteristic P=O stretching vibrations in compound **5-8** are observed as intense signals in the range 1199-1204 cm^{-1}. Further, peaks in the range of 956-992 cm^{-1} and 1039-1047 cm^{-1} corresponds to the symmetric and asymmetric stretching vibration of the PO$_2$ group, respectively.
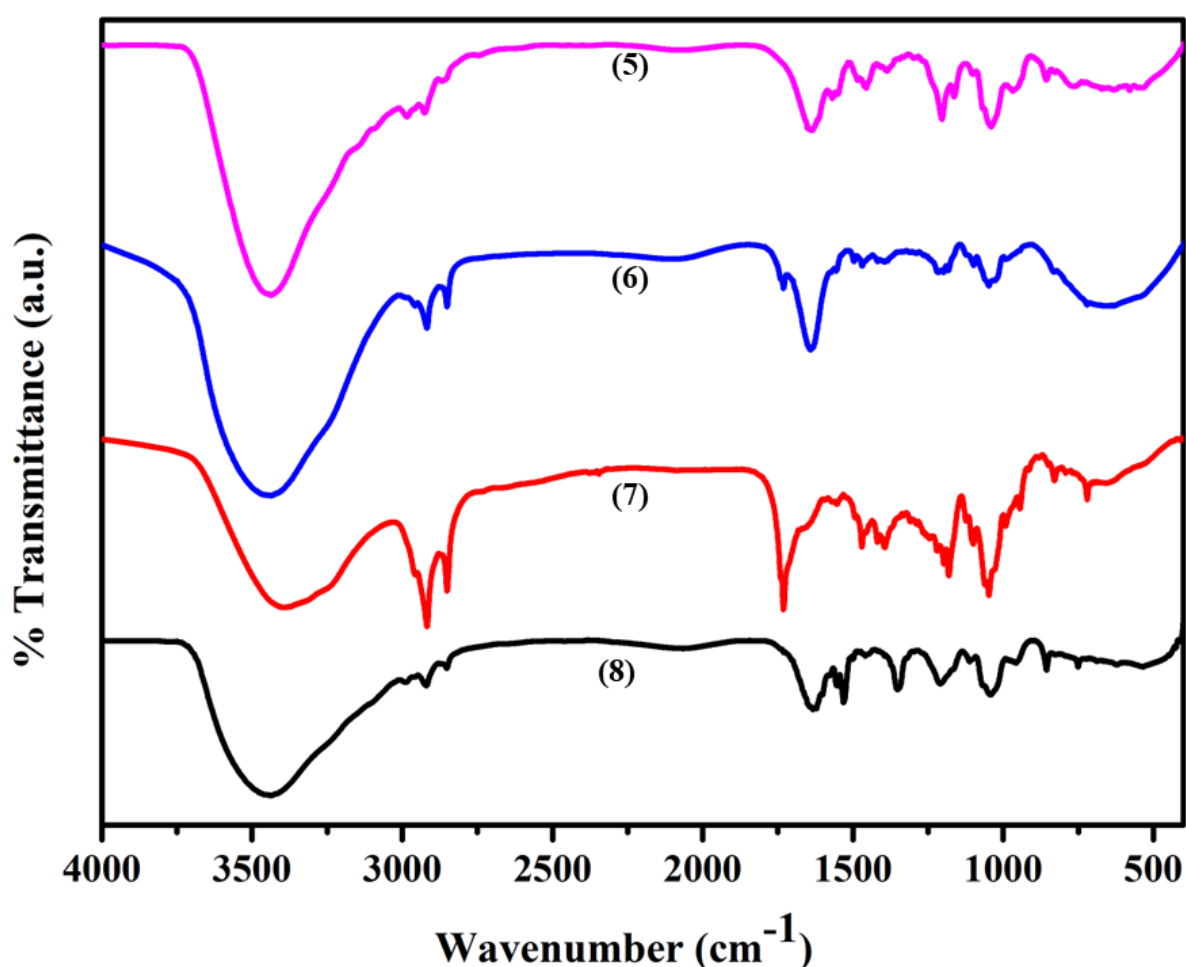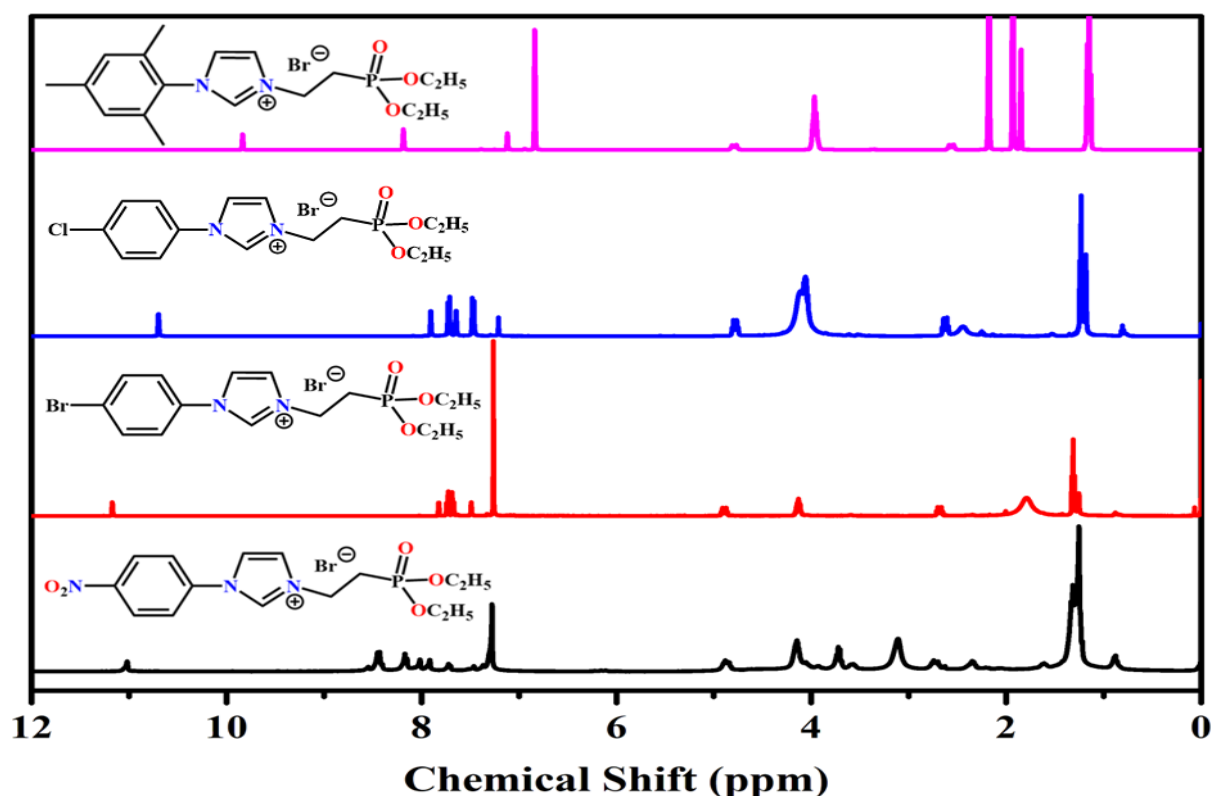

Figure 2.5. FT-IR spectra of Phosphonate ester functionalized imidazolium salts (**5-8**)

The ^{1}H NMR spectra of compound (**5-8**) are depicted in Figure 2.6 and peaks for all constituent protons in **5-8** are observed in expected chemical shift ranges. Aromatic proton attached to imidazole C2 in **5-8** resonate as singlets at δ 9.83, 10.90, 11.17 and 11.02 ppm, respectively. Electronic effects of the remote aromatic substituents present in **5-8** on the

resonances of the imidazole C2 proton are distinctly visible in the ^{1}H NMR spectra. The aromatic proton attached to imidazole C2-atom resonate at considerably downfield region when electron donating mesityl substituent is present as compared to the resonance observed in case of electron withdrawing substituents. The signals for methyl protons on the mesitylene group in **5** are observed as singlets at 2.18 ppm and 1.93 ppm. Aromatic protons in **5**-**8** resonate in the range 6.84-8.43 ppm while the protons associated with the ethylene bridge are observed as multiplets in the range 2.54-4.91 ppm. Further, signals for the protons of the ethyl ester groups **5**-**8** appear in the range of 1.15-4.16 ppm.

Figure 2.6. ^{1}H NMR spectra of phosphonate ester functionalized imidazolium salts (**5**-**8**)

The ^{13}C NMR spectra of **5-8** are depicted in Figure 2.7 and peaks for all constituent carbon atoms in these compounds are observed in expected chemical shift ranges. In case of **5**, the methyl carbon atoms of mesityl group are observed at 17.61 ppm and 21.06 ppm. Peaks observed in the range 129.74-141.11 ppm can be assigned to the aromatic carbon atoms of **5-8** while carbon atoms associated with the ethylene bridge resonate in the range 27.5-44.8 ppm. Further, the signals in the range 16.2-62.7 ppm are perceived to be the characteristics resonances of carbon atoms belonging to the ethyl groups of the phosphonate esters.
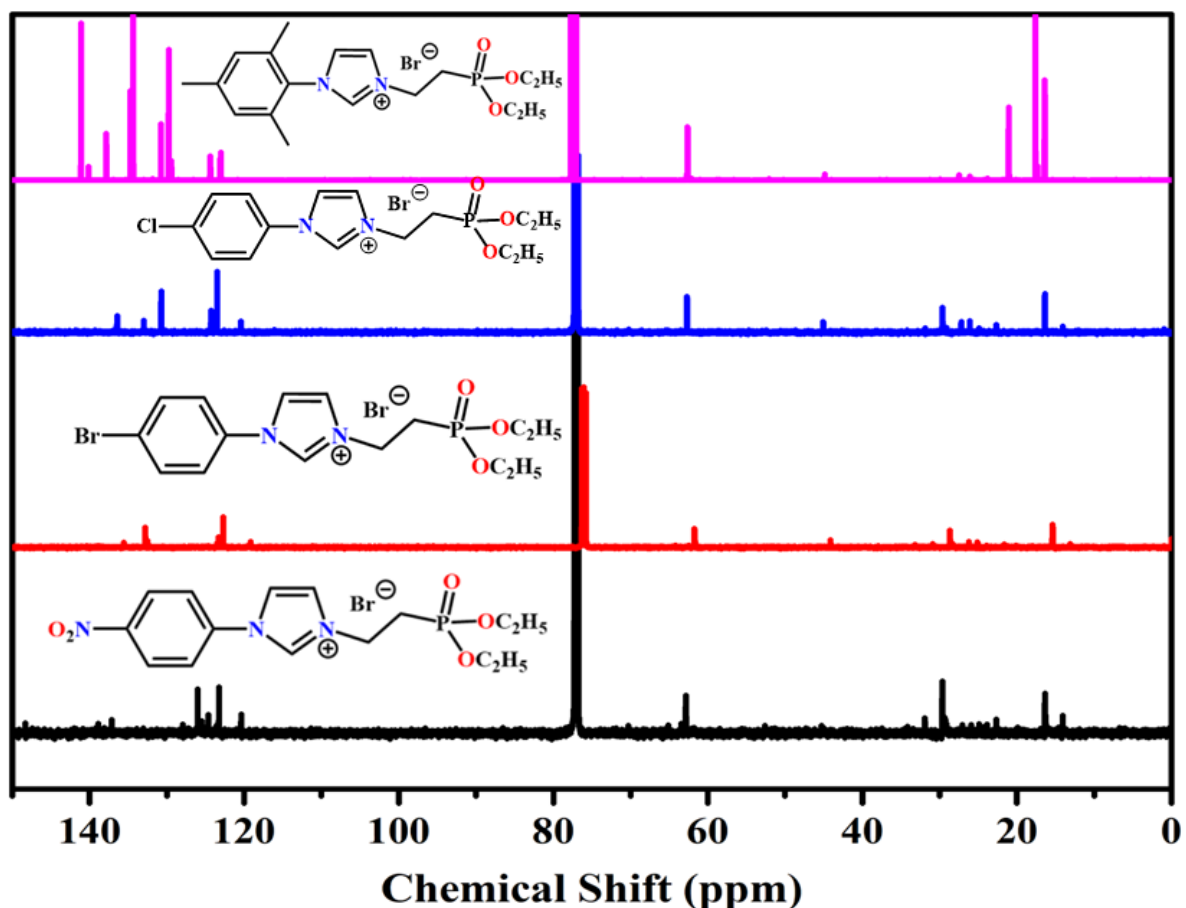
Figure 2.7. ^{13}C NMR spectra of phosphonate ester functionalized imidazolium salts (**5-8**)

^{31}P NMR spectroscopy is a highly sensitive probe to investigate the influence of different substituents on phosphonate esters. The presence of phosphonate ester groups in **5-8** can be confirmed by ^{31}P NMR and the corresponding spectra are depicted in Figure 2.8. ^{31}P NMR spectra of **5-8** show only one peak at δ 26.85, 25.53, 25.53 and 25.39 ppm, respectively and thus confirm the purity of these samples. The ^{31}P NMR chemical shifts values in **5-8** are in good agreement with values observed in spectra of other reported aliphatic phosphonate diesters. Further, ^{31}P NMR spectra of **5-8** reveal the remote influence of the electronic nature of the aromatic substituent on the imidazole ring influences upon the ^{31}P resonance. The ^{31}P resonance of phosphonate esters are observed in a slightly downfield region when electron withdrawing aromatic substituents are present on the imidazole N-atoms.
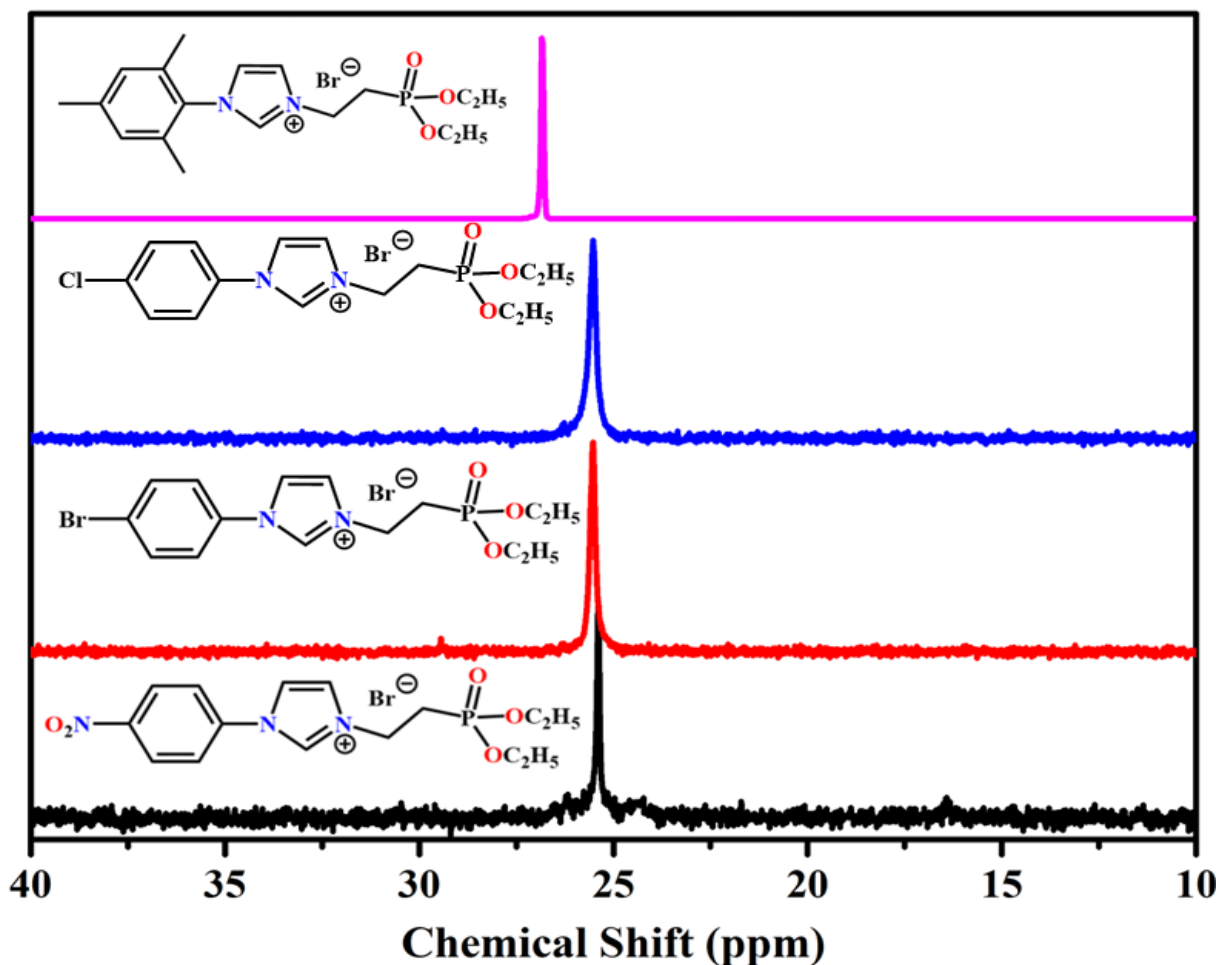
Figure 2.8. ^{31}P NMR spectra of phosphonate ester functionalized imidazolium salts (**5**-**8**)

The high-resolution mass spectrometric (HRMS) fragmentation patterns of compounds **5-8** are depicted in Figure 2.9. Based peaks observed at m/z values 352, 345, 387 and 354 in the HRMS data of **5-8** can be assigned as the respective molecular ion peaks, [M]$^+$ and serve as unequivocal evidence for formation of the title compounds. The mass spectrometric fragmentation patterns of compound **5** and **8** exhibit characteristic peaks for loss of two successive ethyl groups from the phosphonate ester substituents. However, the HRMS fragmentation patterns of compounds **6** and **7** do not show any such peaks for loss of constituent ethyl groups.
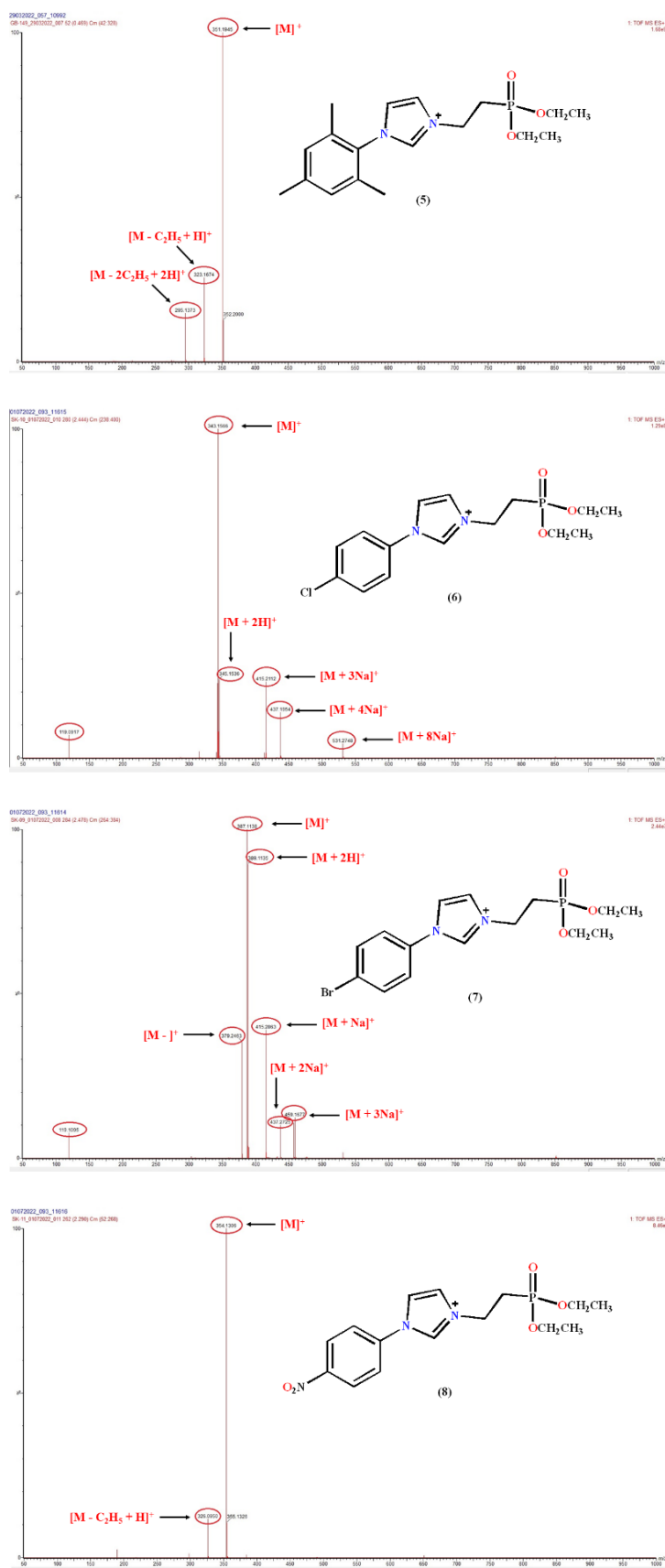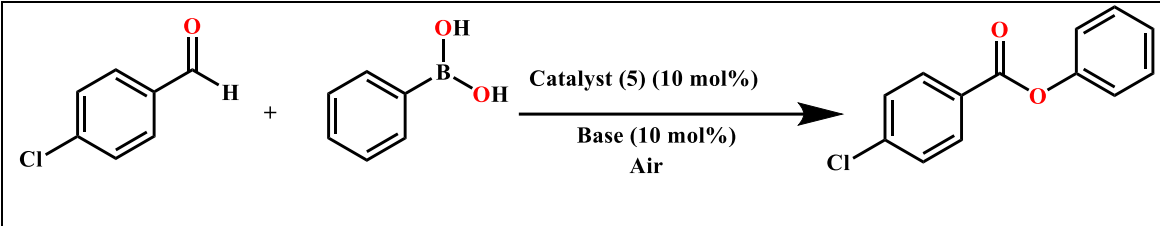
Figure 2.9. High resolution mass spectrometry of phosphonate ester functionalized imidazolium salts (**5**-**8**)

2.4.4. Phosphonate functionalized NHC catalysed esterification of benzaldehydes

NHCs have emerged as a promising green and cost-effective alternative for catalytic application in oxidation processes that involves expensive transition metal catalyst and oxidizing reagent. Catalytic efficacy of NHCs derived from the phosphonate ester functionalized imidazolium salts (**5**-**8**) in esterification of aromatic aldehydes is investigated by employing two different substrates viz. aryl boronic acids and aromatic/aliphatic alcohols. Initially several aldehydes were considered as potential substrates for the intended aerobic esterification reaction. The optimisation study of oxidative esterification reaction was carried out using p-chlorobenzaldehyde and phenyl boronic acid as model substrates and the results are listed in Table 2.3.
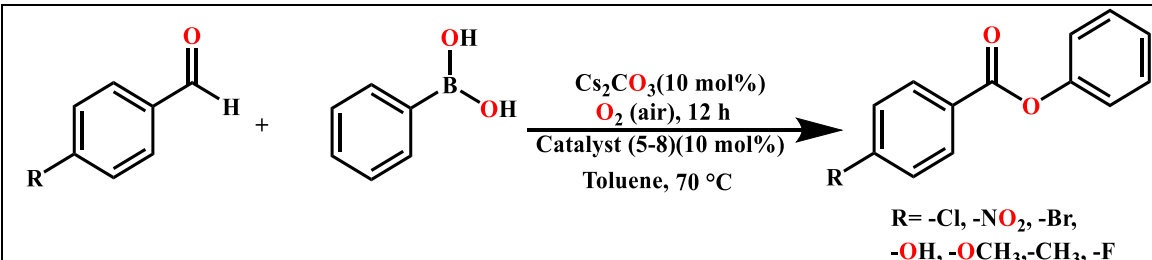
Table 2.3. Optimization of reaction condition for **5** catalysed aerobic esterification of 4-chlorobenzaldehyde with phenyl boronic acid

Solvent	Time (h)	Temperature (°C)	Base (10 mol%)	% Conversion
Toluene	12	RT	Cs_2CO_3	trace
Toluene	12	50	Cs_2CO_3	64
Toluene	12	60	Cs_2CO_3	75
Toluene	12	80	Cs_2CO_3	91
Toluene	12	90	Cs_2CO_3	92
Toluene	2	70	Cs_2CO_3	trace
Toluene	4	70	Cs_2CO_3	20
Toluene	6	70	Cs_2CO_3	52
Toluene	9	70	Cs_2CO_3	70
Toluene	11	70	Cs_2CO_3	88
Toluene	12	70	DBU	20
Toluene	12	70	K_2CO_3	50
Toluene	12	70	$NaHCO_3$	10
Toluene	**12**	**70**	**Cs_2CO_3**	**91**
THF	12	70	Cs_2CO_3	76
1,4-Dioxane	12	70	Cs_2CO_3	25
CH_3CN	12	70	Cs_2CO_3	trace

Initial studies using **5** (10 mol%) as catalyst under aerobic conditions at RT did not result the desired aromatic ester. Progress of the reaction leading to formation of aromatic ester is observed upon increasing the reaction temperature to 50 °C. Based on the above result, optimisation of different reaction conditions e.g. temperature, base, solvent, and time were explored and the % conversion of benzaldehyde into the corresponding aromatic ester under different reaction conditions are listed in Table 2.3. The best % conversion ratio was observed when Cs_2CO_3 is used as the base in toluene medium at 70 °C for a reaction time of 12 h. All other bases investigated *viz.* $NaHCO_3$, DBU and K_2CO_3 did not exhibit reasonable conversion. Moreover, poor conversion was observed when 1,4-Dioxane and CH_3CN were used as solvent medium, though reasonably good conversion is observed in THF medium. Using the above optimized reaction conditions, the substrate scope of the aerobic esterification reaction of benzaldehyde with phenyl boronic acid was explored by employing 10 mol% **5-8** as catalysts (Table 2.4; Figure A1-A24)
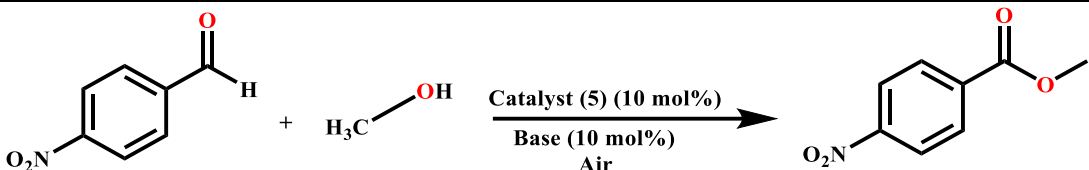
Table 2.4. 5-**8** catalysed esterification of different benzaldehydes with phenyl boronic acid

Sl. No.	-R	% Conversion for different catalyst			
		5	6	7	8
1	-NO$_2$	98	87	88	99
2	-OCH$_3$	94	95	94	99
3	-Br	84	90	84	88
4	-Cl	91	76	71	73
5	-CH$_3$	84	76	70	65
6	-F	77	42	67	99

In most of the cases, good conversion (up to 99%) of the benzaldehydes into the corresponding esters were observed. No appreciable differences in % conversions were observed for different catalyst. This indicate that the electronic nature of the substituents present in the phosphonate functionalized imidazolium salts, **5**-**8** has little bearing in the

catalytic cycle of the esterification reaction. Nonetheless, very good conversions were observed when electron withdrawing substituents are present on the aromatic aldehyde as compared to benzaldehydes containing electron donating substituents. Thereafter, NHC catalysed esterification reaction of different para-substituted aromatic aldehydes with both aliphatic and aromatic alcohols was investigated. Optimization studies was carried out for p-nitrobenzaldehyde and methanol as model substrates (Table 2.5). In this case as well, trace amount of conversion was observed at room temperature while considerable progress of the reaction is observed upon increasing the reaction temperature. The best conversion was observed in THF at 70 °C in 12 hours when Cs_2CO_3 was used as base. Employing $NaHCO_3$ and DBU resulted rather poor conversion while 60 % conversion of p-nitrobenzaldehyde is observed when K_2CO_3 is used as base.
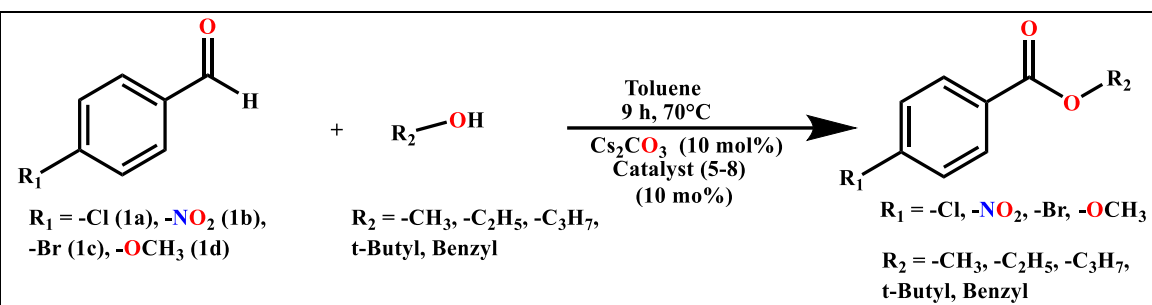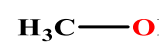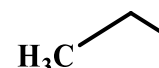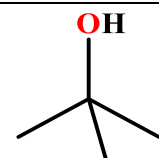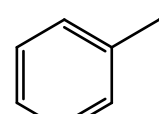
Table 2.5. Optimization of reaction condition for **5** catalysed aerobic esterification of 4-nitrobenzaldehyde with methanol

Solvent	Time (h)	Temperature (°C)	Base (10 mol%)	% Conversion
THF	9	RT	Cs_2CO_3	trace
THF	9	50	Cs_2CO_3	65
THF	9	60	Cs_2CO_3	80
THF	9	80	Cs_2CO_3	95
THF	9	90	Cs_2CO_3	96
THF	1	70	Cs_2CO_3	trace
THF	3	70	Cs_2CO_3	30
THF	5	70	Cs_2CO_3	62
THF	7	70	Cs_2CO_3	80
THF	8	70	Cs_2CO_3	87
THF	9	70	DBU	30
THF	9	70	K_2CO_3	60
THF	9	70	$NaHCO_3$	15
Toluene	**9**	**70**	**Cs_2CO_3**	**93**
THF	**9**	**70**	**Cs_2CO_3**	**95**
1,4-Dioxane	9	70	Cs_2CO_3	25
CH_3CN	9	70	Cs_2CO_3	trace

As observed in case of the esterification reaction involving phenyl boronic acid, in this case also high conversion of benzaldehyde into the corresponding ester is observed in toluene and THF medium while poor conversions are observed in 1,4-Dioxane and CH_3CN mediums.

The above optimized conditions are utilized to explore the esterification reaction of para-substituted benzaldehydes with a series of aliphatic/aromatic alcohols by employing 10% of **5-8** as catalyst (Table 2.6; Figure (A25-A103)). In most of the cases moderate to good (25-99%) conversion of the para-substituted benzaldehyde to the corresponding aromatic ester is observed. As observed in case the earlier esterification reaction, no major differences in

Table 2.6. 5-8 catalysed conversion of different benzaldehydes with alcohols into corresponding esters under optimized reaction condition

Sl. No.	Substrate	Substrate	% Conversion			
			5	**6**	**7**	**8**
1.	H_3C—OH	1a	54	85	64	81
		1b	93	86	98	76
		1c	60	77	87	88
		1d	35	92	93	72
2.	H_3C OH	1a	75	88	80	79
		1b	95	93	95	98
		1c	48	87	90	87
		1d	51	92	93	69
3.	H_3C OH	1a	72	79	79	78
		1b	50	76	90	99
		1c	48	87	90	88
		1d	49	93	25	68
4.	OH	1a	86	79	78	79
		1b	86	88	86	79
		1c	36	85	88	86
		1d	51	93	93	69
5.	OH (benzyl)	1a	70	91	60	77
		1b	96	82	79	80
		1c	44	98	99	99
		1d	35	89	90	68

% conversions of the benzaldehyde are observed for catalyst **5-8**. Further, no clear difference in % conversions were observed even upon changing the electronic nature of substituents present in the para-substituted benzaldehyde. Apart from that, the nature of alcohol also has little bearing in the observed % conversions of benzaldehydes into the corresponding ester.

2.4.5. Computational studies on NHCs derived from **5-8**

Density functional theory calculations were carried out on respective NHC structures (**A-D**) derived from the corresponding phosphonate functionalized imidazolium salts, **5-8**. Optimized structures of singlet-state geometries of all the four NHCs, **A-D** calculated at the B3LYP/6-31+G(d,p) level of theory are depicted in Figure 2.10.
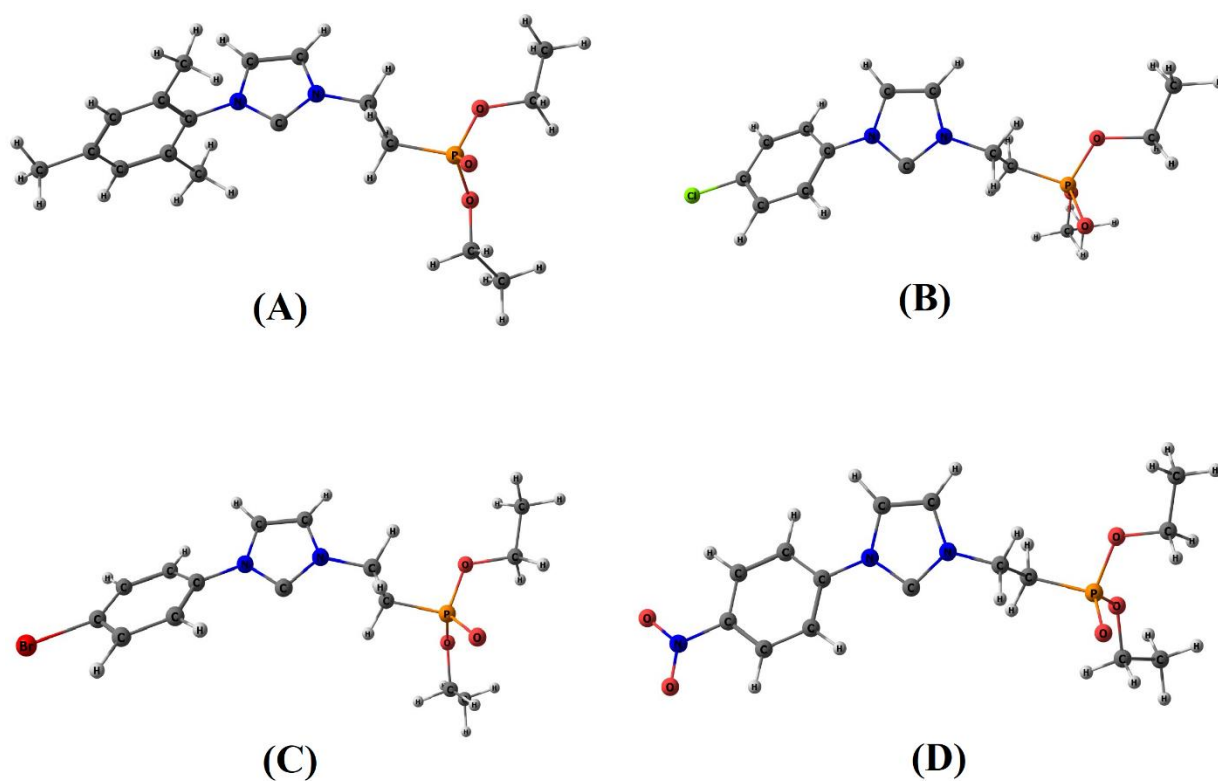

(A)   **(B)**

(C)   **(D)**

Figure 2.10. Optimized structures of singlet-state geometries of all the four NHC's (**A-D**) calculated at the B3LYP/6-31+G(d,p) level of theory

NBO analysis of HOMO, LUMO iso-surfaces in NHCs, **A-D** calculated at the same level of theory is plotted in Figure 2.11. Frequency calculations exhibited absence of imaginary frequencies, which indicated the optimized structures to be true minima on the potential energy surface (PES).
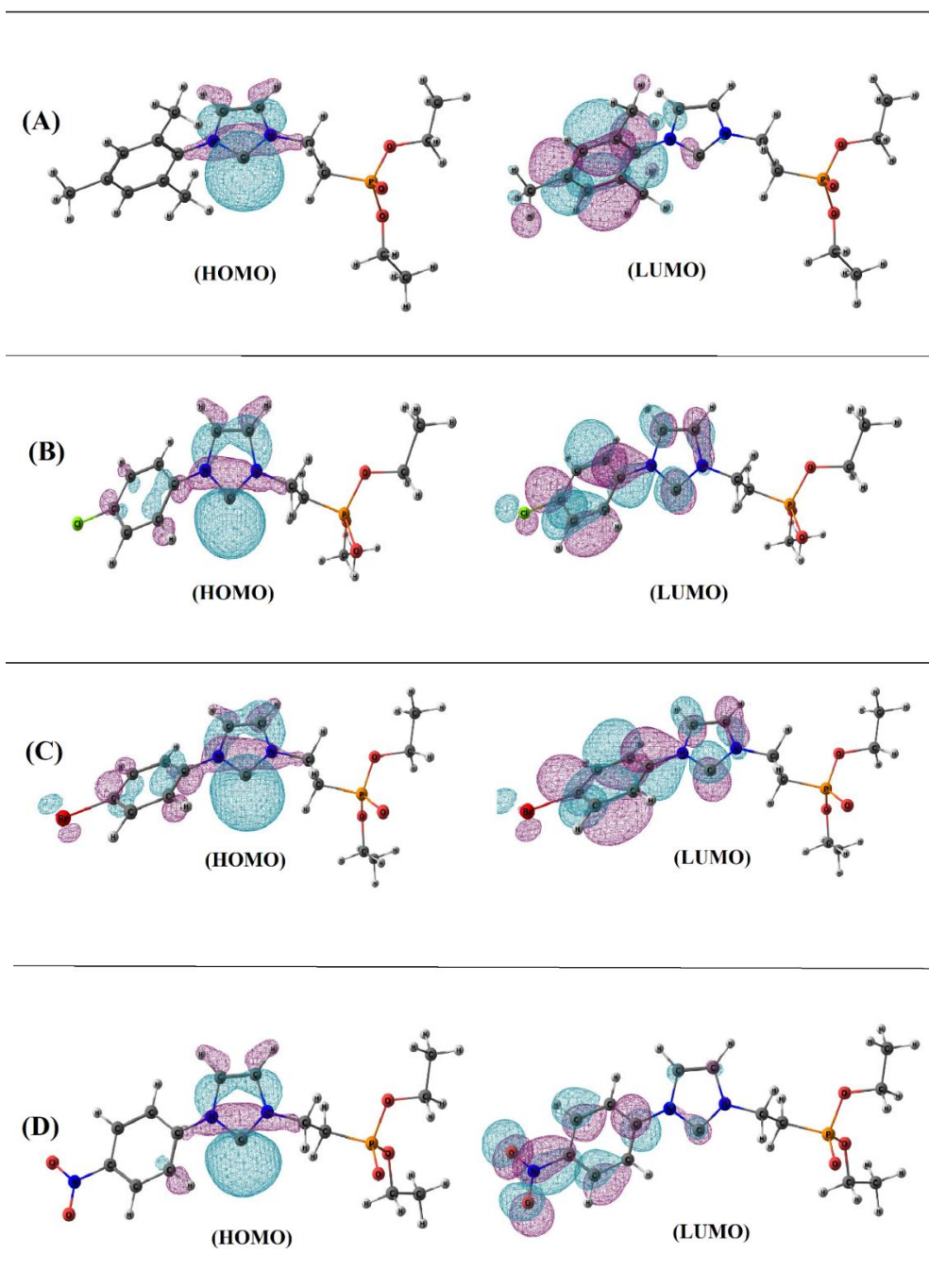
Figure 2.11. HOMO, LUMO iso-surfaces of all the four NHC's (**A**-**D**) calculated at the B3LYP/6-31+G(d,p) level of theory

NHCs **A**-**D** derived from phosphonate functionalized imidazolium salts, **5**-**8** are characterised as singlet carbenes that have σ symmetry for highest occupied Kohn-Sham orbitals with respect to the NHC plane. The E_{HOMO} values are well within the expected range and do not deviate significantly with respect to the substituents R-group. An

inverse correlation exists between the proton affinity of free carbenes and the eigen values of the σ lone pair orbitals (Figure 2.12).
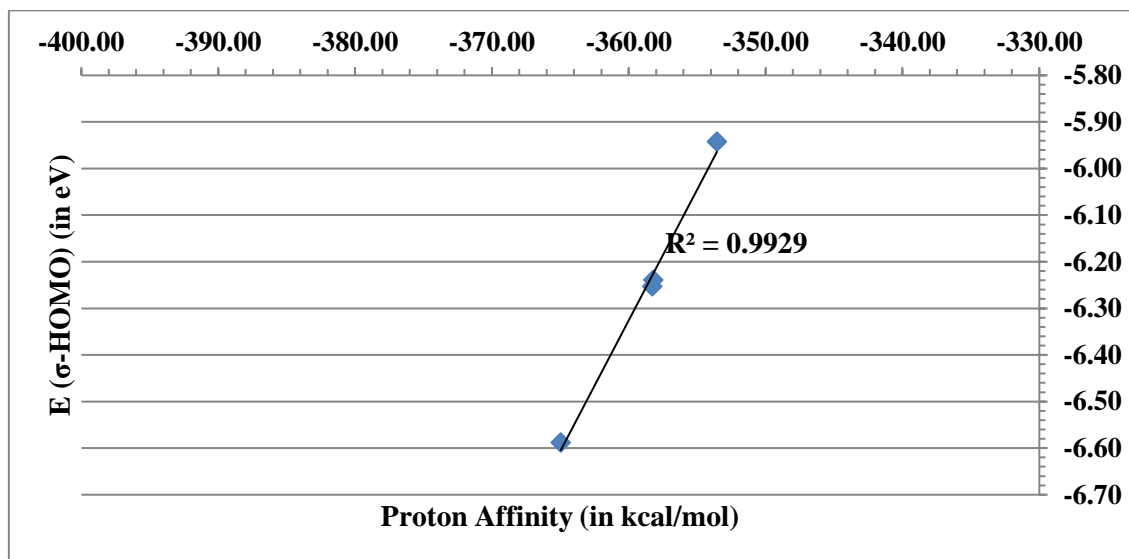

Figure 2.12. Correlation ($R^2=0.9929$) between the proton affinity of free carbenes and the eigenvalues of the σ lone-pair orbital

Since eigen values of σ lone pair orbitals are in correlation with the donor strength of NHCs, **A-D** are ranked according to their proton affinity values and E(σ_{HOMO}) in Table 2.7. Among the considered NHCs, **D** bears the highest proton affinity value. The proton affinities of NHC **B** and **C** are comparable whereas **A** has the least proton affinity value. Similarly, the trend for eigen value for σ orbitals is in the ascending order of catalyst **A**> **B**˜ **C** > **D**, indicating that the most strongly donating one is **A**. The theoretical calculations exhibit good agreement with our experimental spectroscopic results.

Table 2.7. Eigen values of σ lone pair orbitals are in correlation with the donor strength of NHCs (**A-D**), and their proton affinity values and E(σ_{HOMO})

NHC	Singlet State Energy (in Hartree)	Protonated-Singlet State Energy (in Hartree)	E_{HOMO} (in eV)	E_{LUMO} (in eV)	Proton affinity (in Hartree)	Proton affinity (kcal/mol)
5	-1378.39	-1378.95	-5.94	-0.37	-0.56	-353.56
6	-1720.12	-1720.69	-6.24	-0.97	-0.57	-358.21
7	-3831.65	-3832.22	-6.25	-1.01	-0.57	-358.28
8	-1465.02	-1465.60	-6.59	-2.80	-0.58	-364.96

2.4.6. Electronic structures and frequency analysis of the species involved in the NHC catalysed aerobic esterification of benzaldehyde with aryl boronic acid

The proposed mechanism for the esterification of benzaldehyde with phenyl boronic acid involve addition of the carbene catalyst (**I**) to the aldehyde (**II**) resulting in the formation of Breslow intermediate (**IV**). The intermediate **V** and **VII** are formed by the reaction of **IV** with oxygen and phenyl boronic acid **VI**. Intermediate **VII** decomposes rapidly to **VIII** via transfer of the phenyl group to the peroxy linkage and formation of the borate anion. Finally intermediate **VIII** expels the NHC precursor and boric acid to give the corresponding ester product (Scheme 2.5).
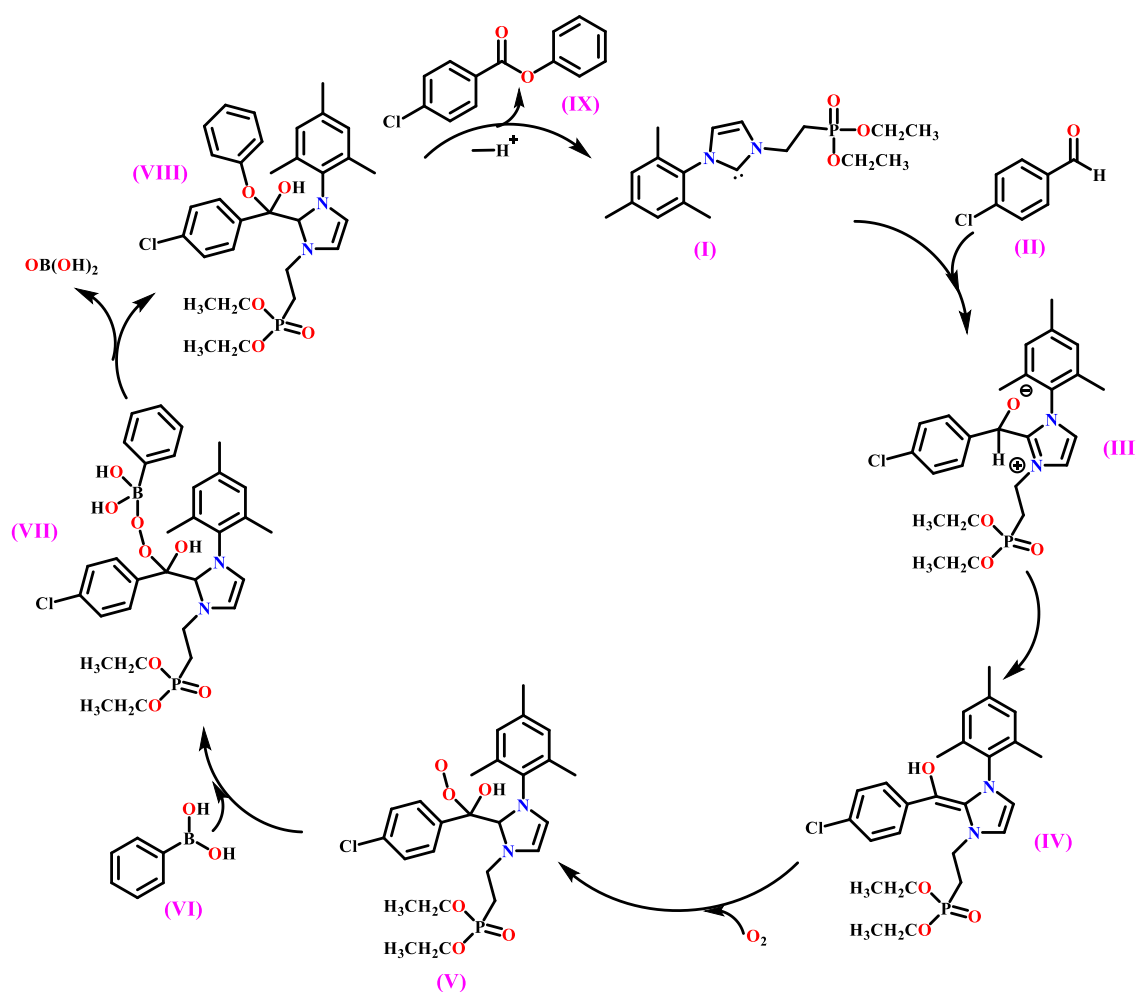
Scheme 2.5. Proposed mechanism for NHC catalysed esterification of benzaldehyde with phenyl boronic acid

The proposed reaction scheme of **A** catalysed aerobic esterification of benzaldehyde with phenyl boronic acid was investigated by performing a detailed theoretical study on all the species involved in the reaction (Scheme 2.5) using the Gaussian09 program

package. Electronic structures of all the stable species of the reactants, products and transition states involved in Scheme 2.5 were optimized using the B3LYP functional along with 6-31G+(d,p) basis set (Figure 2.13). Acetonitrile solvent was used using the conductor-like polarizable continuum model (CPCM) [57] and setting the temperature to 70°C.
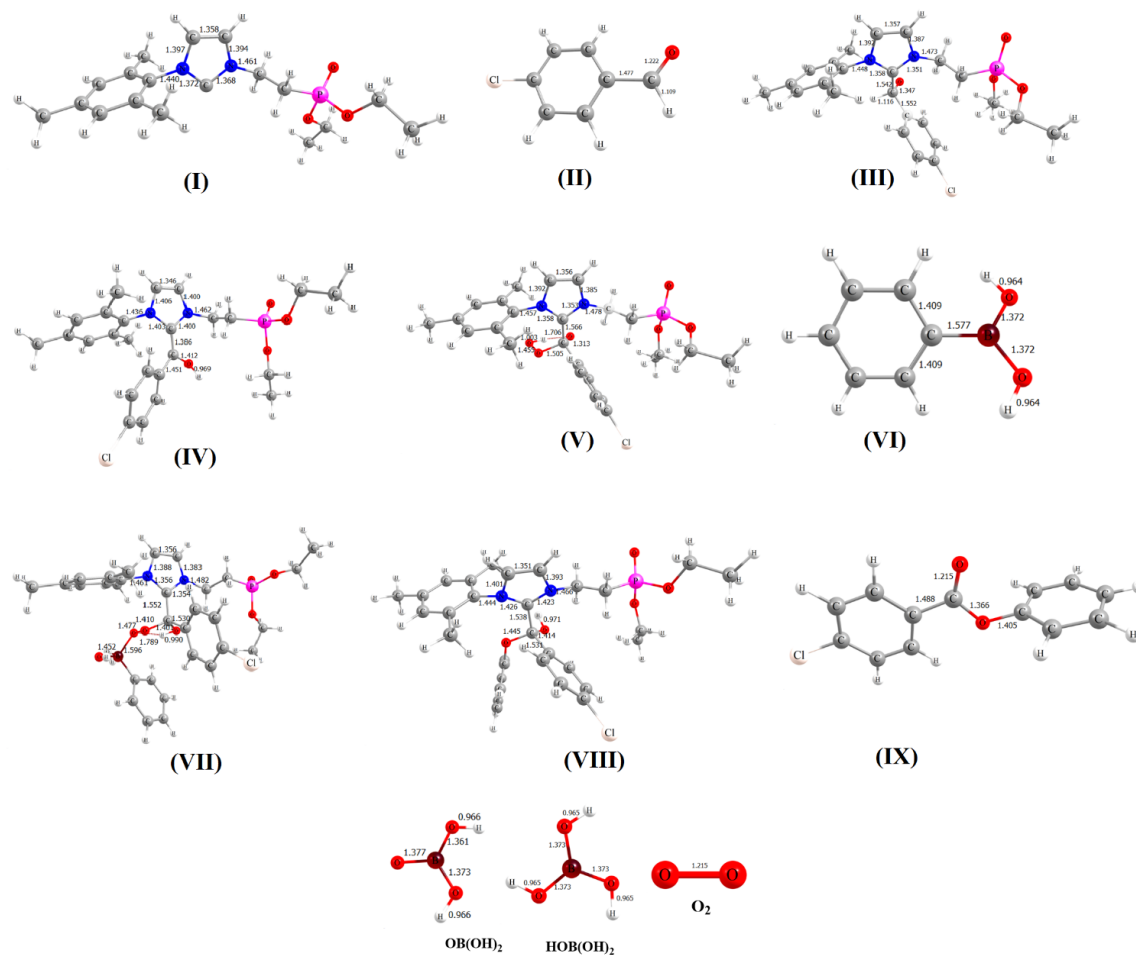

Figure 2.13. Optimized structure of all stable species calculated at B3LYP/6-31+G(d,p) level of theory

Vibrational frequencies calculations were carried out using the same level of theory. All the stationary points have been identified by real positive vibrational frequencies (NMIAG=0) corresponding to stable minima, except the transition state structures (TS's) wherein TS structures were characterized by only one imaginary frequency (NMIAG=1) (Figure 2.14). Intrinsic reaction coordinate (IRC) calculation [58] was also performed to confirm that the transition state properly connected the reactants and the products and

that the transition was smooth which has been discussed in detail in the subsequent sections.
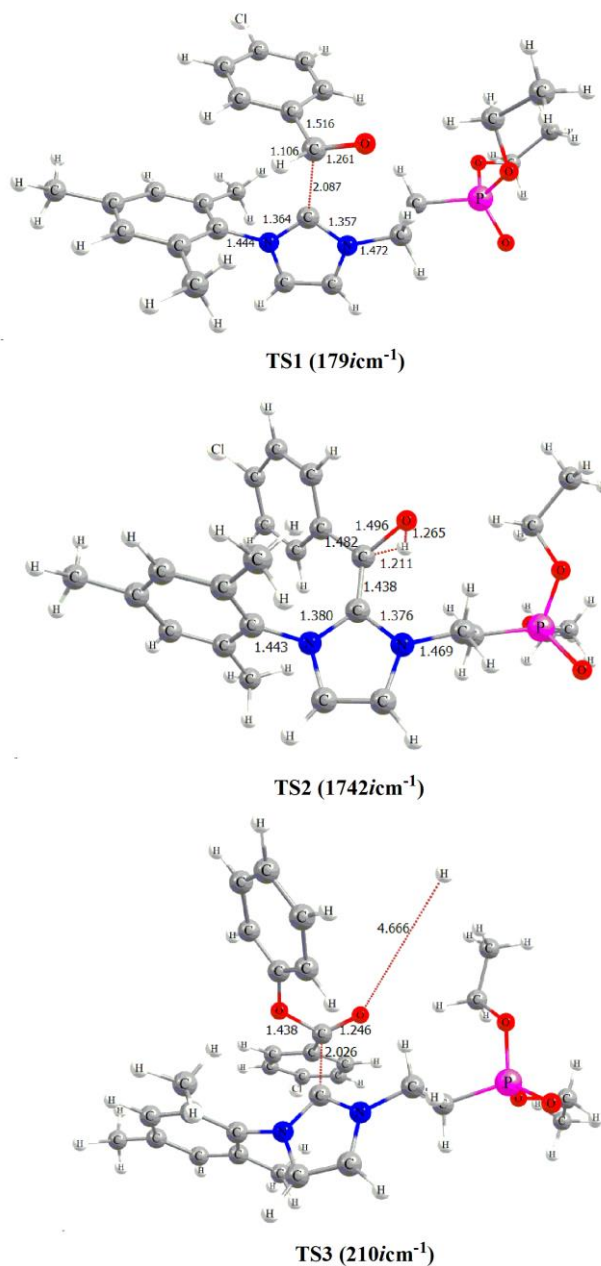

Figure 2.14. Optimized structure of transition states calculated at B3LYP/6-31+G(d,p) level of theory

As we observed from Figure 2.13, the C-atom of –CHO site of **II** bonded with C-atom of –CN site of **I** at a distance of 1.542Å. Each CN bond distances of **II** decreased after bonded with **II** while C-C bond of –C-CHO of **II** increased (from 1.477 Å to 1.522 Å). In **IV** we found that H-atom of –CHO of **III** migrated to O-atom of –CHO and formed a

bond at a distance of 0.969 Å. On the other hand –CP bond of species are found to be 1.412 Å while this distance was 1.347 Å in **III**. In the next introduction of O_2 molecule take place in **IV** (see Figure 2.13) and formed **V**. Here O-O bond was found to be 1.455 Å and at the same time H-atom form a bond with O-atom of O-O at a distance of 1.003 Å. This H-atom also forms a weak H-bond with O-atom of C-C site a distance of 1.706 Å. Further **VI** reacts with **V** and forms **VII**. In **VII**, the distance of B-atom of $B(OH)_2$ site was found to be 1.596 Å with O-atom of O-O site. After removal of $OB(OH)_2$ from **VII**, **VIII** formed. We have also observed some structural changes in **VIII** than **VII**. In the final step, removal of **IX** as well as $HOB(OH)_2$ take place and formed **I**.

It is importance to notify here that, during **I→III**, **III→IV** and **VIII→I**, we have identified transition state structures TS1, TS2 and TS3 as shown in Figure 2.14. We have also given negative frequency of each TSs in this Figure. In TS1, C-C bond was found to be 2.087Å and corresponding C-C vibration frequency was found to be 179 $i$cm^{-1}. In TS2, C-H distance as 1.211 Å and for this bond C-H frequency was found to be 1742 $i$cm^{-1}. In TS3, C-C bond breaking take place and this distance was found to 2.026 Å and in this H-atom –CHO site found a distance of 4.666 Å with O-atom of -CHO site. For this TS, vibration frequency was found to be 210 $i$cm^{-1}.

2.4.7. Thermochemistry and PES analysis

From frequency calculations, thermo-chemical data were obtained and from these data we determined the standard reaction enthalpy ($\Delta_r H^0$) and Gibbs free energy ($\Delta_r G^0$) for the reaction steps and these values are listed in Table 2.8. It has been observed from Table 2.8 that **I** converted into **III** in the presence of **II** (4-chlorobenaldehyde), and the value of $\Delta_r H^o$ and $\Delta_r G^o$ were found to have positive value which implies that this step is slightly endothermic and non-spontaneous. In the next step (**III→IV**), the values of $\Delta_r H^o$ and $\Delta_r G^o$ are less than zero which indicates that this step is exothermic and a spontaneous process. Next, in the presence of O_2, **IV** converted into **V** in which the reaction is more exothermic and spontaneous than the previous step. Further **V**+**VI**→**VII** reaction shows that the reaction is exothermic but nonspontaneous while **VII**→**VIII**+$OB(OH)_2$ reaction shows that reaction is spontaneous. The last step of the reaction shows that it is highly exothermic and highly spontaneous.

Table 2.8: Standard enthalpy and Gibbs free energy changes (in kcal mol^{-1}) of reaction steps calculated at B3LYP/6-31+G(d,p) level of theory

Reaction Channels	Thermo-chemistry	
	$\Delta_r H^o$	$\Delta_r G^o$
I+**II**→**III**	5.54	22.86
III→**IV**	-2.46	-2.61
IV + O$_2$→**V**	-25.51	-11.16
V+ **VI**→**VII**	-5.08	8.99
VII→**VIII**+OB(OH)$_2$	2.69	-14.30
VIII+OB(OH)$_2$→**IX**+OHB(OH)$_2$+**I**	-94.92	-111.15

We have explored all the reaction steps involved in the proposed reaction mechanism on the potential energy surface (PES) as shown in Figure 2.15. It is obvious from Figure 2.15, during the conversion of **I**→**III**, a barrier height of TS1 was found to be 8.83 kcal
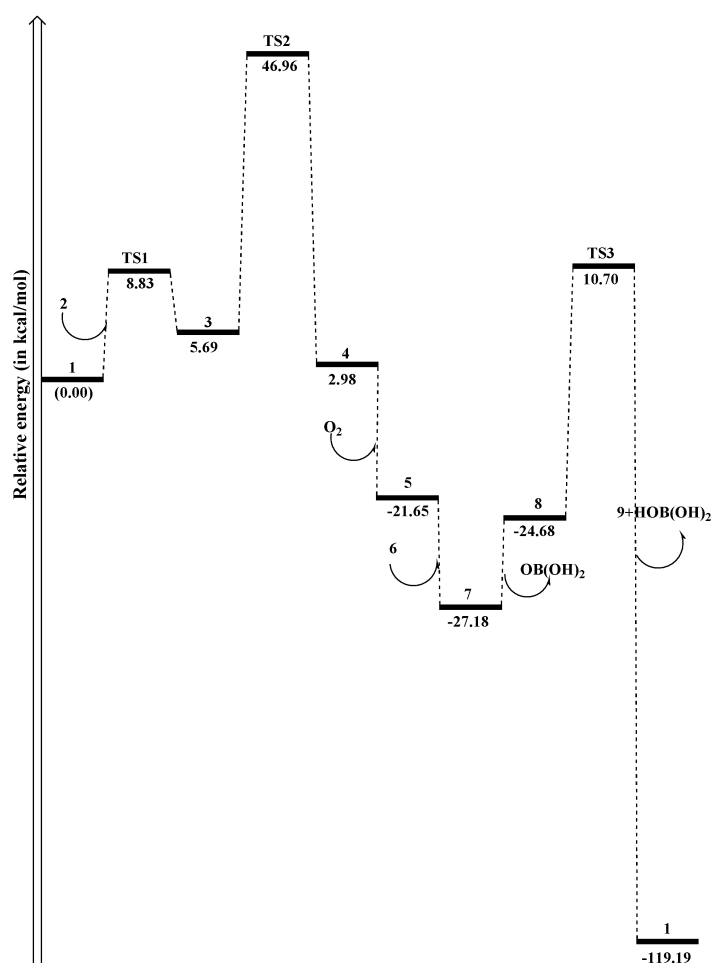

Figure 2.15. Potential energy diagram of proposed reaction at B3LYP/6-31+G(d,p) level of theory

mol^{-1} and the energy of **III** relative to TS1 was found to be -3.14 kcal mol^{-1}. The energy barrier for TS2 was 41.27 kcal mol^{-1} relative to **III** and corresponding **IV** has energy -43.98 kcal mol^{-1} relative to TS2. In the next step, addition of O$_2$ take place in **IV** and was found that energy of **V** becomes -24.63 kcal mol^{-1} relative to **IV**. Further, **VI** on addition to **V** yields **VII** and energy of **VII** was found to be -5.53 kcal mol^{-1} relative to **V**. Now OB(OH)$_2$ added to **VII** yields **VIII** which has energy 2.50 kcal mol^{-1} relative to **VII**. In the last step (**VIII→I**), energy barrier of TS3 was found to be 35.38 kcal mol^{-1}. In this step energy of **I** was found to be -129.89 kcal mol^{-1} relative to TS3. Thus, we find that from PES diagram that the proposed reaction mechanism is a possible one on the basis of theoretical finding.

2.5. Conclusions

Starting from N-aryl substituted imidazole's, a series of phosphonate ester functionalized imidazolium salts are prepared and characterized during this chapter. Thus, we have developed a straightforward preparative approach for the synthesis of four phosphonate functionalised imidazolium salts and they are characterized by using FT-IR, ^{1}H NMR, ^{13}C NMR, ^{31}P NMR and HRMS techniques. The NHCs derived from the phosphonate functionalized imidazolium salts act as efficient organocatalysts in aerobic esterification of benzaldehyde with two different substrates viz. phenyl boronic acid and aliphatic/benzyl alcohol. Further, DFT calculations were carried out to evaluate the electronic characteristics of the NHCs derived from the phosphonate functionalized imidazolium salts prepared during this study. The mechanism of the phosphonate functionalized NHC catalysed aerobic esterification of benzaldehyde phenyl boronic acid was also probed by using DFT calculations.

NHCs are workhorses in organic and organometallic chemistry, competing with phosphines as auxiliary ligands in transition metal catalysis and opening new avenues in main-group chemistry and organocatalysis. The unique ability of NHCs to reverse the reactivity of carbonyl carbon atom via formation of Breslow intermediate has opened immense possibilities for their application in organocatalysis. However, presence of bulky electron donating aromatic substituents on the imidazolium N atoms remains important criteria that must be fulfilled to enhance the electron donation characteristics of the NHCs for formation of Breslow intermediate. The present study established that phosphonate group can enhance the catalytic activity so that even NHCs with small

aliphatic substituents can also show high catalytic efficacy. This study has thus opened fascinating frontiers for augmenting organocatalytic efficacy of NHCs by introducing additional functional groups.

2.6. References

[1]   Enders, D., Niemeier, O., and Henseler, A. Organocatalysis by N-heterocyclic carbenes. *Chemical Reviews*, 107(12):5606-5655, 2007.

[2]   Ukai, M., Pinaud, J., Gnanou, Y., Vignolle, J., and Taton, D. N-Heterocyclic carbenes (NHCs) as organocatalysts and structural components in metal-free polymer synthesis. *Chemical Society Reviews*, 42(5):2142-2172, 2013.

[3]   Ukai, T., Tanaka, R., and Dokawa, T. A new catalyst for acyloin condensation. *Journal of the Pharmaceutical Society of Japan*, 63:296-300, 1943.

[4]   Breslow, R. On the mechanism of thiamine action. IV. 1 Evidence from studies on model systems. *Journal of the American Chemical Society*, 80(14):3719-3726, 1958.

[5]   Bugaut, X. and Glorius, F. Organocatalytic umpolung: N-heterocyclic carbenes and beyond. *Chemical Society Reviews*, 41(9):3511-3522, 2012.

[6]   Ryan, S.J., Candish, L., and Lupton, D.W. Acyl anion free N-heterocyclic carbene organocatalysis. *Chemical Society Reviews*, 42(12):4906-4917, 2013.

[7]   Biju, A.T., Kuhl, N., and Glorius, F. Extending NHC-catalysis: coupling aldehydes with unconventional reaction partners. *Accounts of chemical research*, 44(11):1182-1195, 2011.

[8]   Schedler, M., Wang, D.S., and Glorius, F. NHC-Catalyzed Hydroacylation of Styrenes. *Angewandte Chemie International Edition*, 52(9):2585-2589, 2013.

[9]   Vora, H.U., Wheeler, P., and Rovis, T. Exploiting Acyl and Enol Azolium Intermediates via N-Hetero-cyclic Carbene-Catalyzed Reactions of α-Reducible Aldehydes. *Advanced synthesis & catalysis*, 354(9):1617-1639, 2012.

[10]   Nair, V., Menon, R.S., Biju, A.T., Sinu, C.R., Paul, R.R., Jose, A., and Sreekumar, V. Employing homoenolates generated by NHC catalysis in carbon–carbon bond-forming reactions: state of the art. *Chemical Society Reviews*, 40(11):5336-5346, 2011.

[11]   Murauski, K.J., Jaworski, A.A., and Scheidt, K.A. A continuing challenge: N-heterocyclic carbene-catalyzed syntheses of γ-butyrolactones. *Chemical Society Reviews*, 47(5):1773-1782, 2018.

[12] Wang, M.H. and Scheidt, K.A. Cooperative Catalysis and Activation with N-Heterocyclic Carbenes. *Angewandte Chemie International Edition*, 55(48):14912-14922, 2016.

[13] Flanigan, D.M., Romanov-Michailidis, F., White, N.A., and Rovis, T. Organocatalytic reactions enabled by N-heterocyclic carbenes. *Chemical Reviews*, 115(17):9307-9387, 2015.

[14] Hopkinson, M.N., Richter, C., Schedler, M., and Glorius, F. An overview of N-heterocyclic carbenes. *Nature*, 510(7506):485-496, 2014.

[15] Mahatthananchai, J. and Bode, J.W. On the mechanism of N-heterocyclic carbene-catalyzed reactions involving acyl azoliums. *Accounts of chemical research*, 47(2):696-707, 2014.

[16] Grossmann, A. and Enders, D., N-heterocyclic carbene catalyzed domino reactions. *Angewandte Chemie International Edition*, 51(2):314-325, 2012.

[17] Cohen, D.T. and Scheidt, K.A., Cooperative Lewis acid/N-heterocyclic carbene catalysis. *Chemical science*, 3(1):53-57, 2012.

[18] Izquierdo, J., Hutson, G.E., Cohen, D.T. and Scheidt, K.A., A Continuum of Progress: Applications of N-Hetereocyclic Carbene Catalysis in Total Synthesis. *Angewandte Chemie International Edition*, 51(47):11686-11698, 2012.

[19] Menon, R.S., Biju, A.T., and Nair, V. Recent advances in N-heterocyclic carbene (NHC)-catalysed benzoin reactions. *Beilstein Journal of Organic Chemistry*, 12(1):444-461, 2016.

[20] Bugaut, X. Benzoin and Aza-benzoin. *Comprehensive Organic Synthesis II*, 424-470, 2014.

[21] Enders, D. and Balensiefer, T. Nucleophilic carbenes in asymmetric organocatalysis. *Accounts of chemical research*, *37*(8):534-541, 2004.

[22] Yetra, S.R., Patra, A., and Biju, A.T. Recent advances in the N-heterocyclic carbene (NHC)-organocatalyzed Stetter reaction and related chemistry. *Synthesis*, 47(10):1357-1378, 2015.

[23] de Alaniz, J.R. and Rovis, T. The catalytic asymmetric intramolecular Stetter reaction. *Synlett*, 2009(08):1189-1207, 2009.

[24] Rovis, T. Development of chiral bicyclic triazolium salt organic catalysts: the importance of the N-aryl substituent. *Chemistry letters*, 37(1):2-7, 2008.

[25] Christmann, M. New developments in the asymmetric Stetter reaction. *Angewandte Chemie International Edition*, 44(18):2632-2634, 2005.

[26] de Alaniz, J.R., Kerr, M.S., Moore, J.L., and Rovis, T. Scope of the asymmetric intramolecular Stetter reaction catalyzed by chiral nucleophilic triazolinylidene carbenes. *The Journal of organic chemistry*, 73(6):2033-2040, 2008.

[27] Stetter, H. Catalyzed addition of aldehydes to activated double bonds—a new synthetic approach. *Angewandte Chemie International Edition in English*, 15(11):639-647, 1976.

[28] Miyashita, A., Suzuki, Y., Nagasaki, I., ISHIGURO, C., IWAMOTO, K.I., and HIGASHINO, T. Catalytic action of azolium salts. VIII. Oxidative aroylation with arenecarbaldehydes catalyzed by 1, 3-dimethylbenzimidazolium iodide. Chemical and pharmaceutical bulletin, 45(8):1254-1258, 1997.

[29] Maki, B.E. and Scheidt, K.A. N-heterocyclic carbene-catalyzed oxidation of unactivated aldehydes to esters. *Organic letters*, 10(19):4331.

[30] Harnying, W., Sudkaow, P., Biswas, A., and Berkessel, A. N-Heterocyclic Carbene/Carboxylic Acid Co-Catalysis Enables Oxidative Esterification of Demanding Aldehydes/Enals, at Low Catalyst Loading. *Angewandte Chemie International Edition*, 60(36):19631-19636, 2021.

[31] Zhang, M., Zhang, S., Zhang, G., Chen, F., and Cheng, J. Palladium/NHC-catalyzed oxidative esterification of aldehydes with phenols. *Tetrahedron Letters*, 52(19):2480-2483, 2011.

[32] Delany, E.G., Fagan, C.L., Gundala, S., Mari, A., Broja, T., Zeitler, K., and Connon, S.J. NHC-catalysed aerobic aldehyde-esterifications with alcohols: no additives or cocatalysts required. *Chemical Communications*, 49(58):6510-6512, 2013.

[33] Reddy, R.S., Rosa, J.N., Veiros, L.F., Caddick, S., and Gois, P.M. NHC/Iron cooperative catalysis: aerobic oxidative esterification of aldehydes with phenols. *Organic & Biomolecular Chemistry*, 9(9):3126-3129, 2011.

[34] De Sarkar, S., Grimme, S., and Studer, A. NHC catalyzed oxidations of aldehydes to esters: chemoselective acylation of alcohols in presence of amines. *Journal of the American Chemical Society*, 132(4):1190-1191, 2010.

[35] Rosa, J.N., Reddy, R.S., Candeias, N.R., Cal, P.M., and Gois, P.M. NHC− Iron-Catalyzed aerobic oxidative aromatic esterification of aldehydes using boronic acids. *Organic Letters*, 12(12):2686-2689, 2010.

[36] Delany, E.G., Fagan, C.L., Gundala, S., Zeitler, K., and Connon, S.J. Aerobic oxidation of NHC-catalysed aldehyde esterifications with alcohols: benzoin, not the Breslow intermediate, undergoes oxidation. *Chemical Communications*, 49(58):6513-6515, 2013.

[37] Maji, B., Vedachalan, S., Ge, X., Cai, S., and Liu, X.W. N-heterocyclic carbene-mediated oxidative esterification of aldehydes: ester formation and mechanistic studies. *The Journal of Organic Chemistry*, 76(9):3016-3023, 2011.

[38] Noonan, C., Baragwanath, L., and Connon, S.J. Nucleophilic carbene-catalysed oxidative esterification reactions. *Tetrahedron Letters*, 49(25):4003-4006, 2008.

[39] Tang, S., Yuan, J., Liu, C., and Lei, A. Direct oxidative esterification of alcohols. *Dalton Transactions*, 43(36):13460-13470, 2014.

[40] Khan, Z., Javed, F., Shamair, Z., Hafeez, A., Fazal, T., Aslam, A., Zimmerman, W.B., and Rehman, F. Current developments in esterification reaction: A review on process and parameters. *Journal of Industrial and Engineering Chemistry*, 103:80-101, 2021.

[41] Kiran, I.C., Lalwani, K., and Sudalai, A. N-Heterocyclic carbene catalyzed esterification of aromatic aldehydes with alcohols under aerobic conditions. *RSC advances*, 3(6):1695-1698, 2013.

[42] Ekoue-Kovi, K. and Wolf, C. One-pot oxidative esterification and amidation of aldehydes. *Chemistry–A European Journal*, 14(21):6302-6315, 2008.

[43] Gaspa, S., Porcheddu, A., and De Luca, L. Recent developments in oxidative esterification and amidation of aldehydes. *Tetrahedron Letters*, 57(31):3433-3440, 2016.

[44] Dzieszkowski, K. and Rafiński, Z. N-Heterocyclic Carbene Catalysis under Oxidizing Conditions. *Catalysts*, 8(11):549, 2018.

[45] Lin, L., Li, Y., Du, W., and Deng, W.P. The NHCs-mediated cross-coupling of aromatic aldehydes with benzyl halides: synthesis of α-aryl ketones. *Tetrahedron Letters*, 51(27):3571-3574, 2010.

[46] Maji, B., Vedachalan, S., Ge, X., Cai, S. and Liu, X.W., N-heterocyclic carbene-mediated oxidative esterification of aldehydes: ester formation and mechanistic studies. *The Journal of Organic Chemistry*, 76(9):3016-3023, 2011.

[47] Maki, B.E. and Scheidt, K.A. N-heterocyclic carbene-catalyzed oxidation of unactivated aldehydes to esters. *Organic letters*, 10(19):4331-4334, 2008.

[48] Kang, Y.W. and Jang, H.Y. NHC-catalyzed one-pot oxidation and oxidative esterification of allylic alcohols using TEMPO: the effect of alcohol additives. *RSC Advances*, 4(84):44486-44490, 2014.

[49] Zhao, J., Mueck-Lichtenfeld, C., and Studer, A. Cooperative N-Heterocyclic Carbene (NHC) and Ruthenium Redox Catalysis: Oxidative Esterification of Aldehydes with Air as the Terminal Oxidant. *Advanced Synthesis & Catalysis*, 355(6):1098-1106, 2013.

[50] Maki, B.E., Chan, A., Phillips, E.M., and Scheidt, K.A. Tandem oxidation of allylic and benzylic alcohols to esters catalyzed by N-heterocyclic carbenes. *Organic Letters*, 9(2):371-374, 2007.

[51] Kühl, O. *Functionalised N-heterocyclic carbene complexes*. John Wiley & Sons, 2010.

[52] Sheldrick, G.M. A short history of SHELX. Acta Crystallographica Section A: *Foundations of Crystallography*, 64(1):112-122, 2008.

[53] Ruddlesden, A.J., Mewis, R.E., Green, G.G., Whitwood, A.C., and Duckett, S.B. Catalytic transfer of magnetism using a neutral iridium phenoxide complex. *Organometallics*, 34(12):2997-3006, 2015.

[54] Frisch, M.J.E.A., Trucks, G.W., Schlegel, H.B., Scuseria, G.E., Robb, M.A., Cheeseman, J.R., Scalmani, G., Barone, V., Mennucci, B., Petersson, G. and Nakatsuji, H., 2009. gaussian 09, Revision d. 01, Gaussian. Inc., Wallingford CT, 201.

[55]   Tirado-Rives, J. and Jorgensen, W.L. Performance of B3LYP density functional methods for a large set of organic molecules. *Journal of chemical theory and computation*, 4(2):297-306, 2008.

[56]   Del Bene, J.E., Person, W.B., and Szczepaniak, K. Properties of Hydrogen-Bonded Complexes Obtained from the B3LYP Functional with 6-31G (d, p) and 6-31+ G (d, p) Basis Sets: Comparison with MP2/6-31+ G (d, p) Results and Experimental Data. *The Journal of Physical Chemistry*, 99(27):10705-10707, 1995.

[57]   Barone, V. and Cossi, M. Quantum calculation of molecular energies and energy gradients in solution by a conductor solvent model. *The Journal of Physical Chemistry A*, 102(11):1995-2001, 1998.

[58]   Gonzalez, C. and Schlegel, H.B. Reaction path following in mass-weighted internal coordinates. *Journal of Physical Chemistry*, 94(14):5523-5527, 1990.